THE ASTROPHYSICAL JOURNAL, 477:631–660, 1997 March 10

INFRARED SPECTROSCOPY OF SEYFERT 2 GALAXIES: A LOOK THROUGH THE OBSCURING TORUS? II.

SYLVAIN VEILLEUX,[1,2] ROBERT W. GOODRICH,[2,3] AND GARY J. HILL[2,4]
Received 1996 June 21; accepted 1996 October 4

ABSTRACT

High-resolution *J*-band and *K*-band spectra of a sample of 33 Seyfert 2 galaxies are presented. Two of these galaxies were also observed in the *L* band. These data are used to look for broad Paβ, Brγ, and Brα lines, in search of broad-line regions (BLRs) that are hidden by dust at optical wavelengths. Obscured BLRs are confirmed for three previously reported discoveries, and the new data suggest possible BLR detections in as many as six additional Seyfert 2's. Our results are consistent with the standard torus model if the transition zone located between the optically thin "throat" of the torus and the optically thick core is rather extended. The dusty wind model of Königl & Kartje can also explain the data.

Comparisons of the broad-line and narrow-line extinctions indicate that the BLRs are considerably more obscured than the narrow-line regions (NLRs). This result agrees with the predictions of both the torus and dusty wind models, where the dust is located between the NLR and the BLR. Comparisons of the column depths to the BLRs with the column depths determined from X-ray data show a general tendency for the objects with detected broad recombination lines to have lower X-ray columns. A large scatter exists between the infrared and X-ray columns depths, however. Fluctuations in the properties of the nuclear gas (e.g., metallicity or gas-to-dust ratio) or differences in the distributions of the ionized and neutral gas components can easily account for this scatter.

The widths of broad Paβ and Brγ lie on the narrow end of the distribution for Seyfert 1 galaxies. The dereddened broad Hβ luminosities predicted from the broad infrared lines are similar to the broad Hβ luminosities of normal Seyfert 1's, and so are the ratios of the hard X-ray flux to the predicted broad Hα flux. In objects with a BLR detected through both infrared spectroscopy and spectropolarimetry, the broad infrared lines often are an order of magnitude stronger than the values expected from the scattered flux.

The infrared spectra were also used to assess the origin of the [Fe II] and H_2 emission in Seyfert 2 galaxies. The present data rule out the possibility that the [Fe II] emission is produced solely from a circumnuclear starburst. Shocks associated with nuclear outflows are a likely source of both [Fe II] and H_2, although photoionization by the nuclear continuum may also contribute to the [Fe II] emission, and X-ray heating may play a role in producing the H_2 emission.

Subject headings: galaxies: ISM — galaxies: photometry — galaxies: Seyfert — infrared: galaxies — X-rays: galaxies

1. INTRODUCTION

When it comes to active galaxies, appearance can sometimes be very deceiving. Over the last decade, evidence has mounted that obscuring material near the cores of active galaxies may conceal the true identity of some of these objects (see, e.g., Lawrence & Elvis 1982). Spectropolarimetric studies have revealed that broad hydrogen recombination lines similar to those in Seyfert 1 galaxies are sometimes observed in the polarized, scattered light of galaxies that would otherwise be classified as Seyfert 2 galaxies (see, e.g., Antonucci & Miller 1985). These data are best explained if the broad-line regions (BLRs) near the centers of these galaxies are hidden from direct view by optically thick material lying along our line of sight, while fine particles located above and below the obscuring mass distribution act as mirrors, scattering light from the BLRs into our line of sight and allowing us to get an indirect peek at the BLRs. In Seyfert 1 galaxies, on the other hand, our vantage point in space is such that the line of sight to the BLR is not significantly attenuated by this obscuring material. A generalization of this idea to all Seyfert galaxies—the so-called Seyfert unification theory—postulates that the viewing angle is the only parameter of importance in determining the appearance of *all* Seyfert galaxies. Much of the recent work in the field of active galactic nuclei (AGNs) has concentrated on testing this theory.

The current spectropolarimetric data seem to fall short in proving that all Seyfert 2 galaxies are actually "hidden Seyfert 1" galaxies (see, e.g., Miller & Goodrich 1990; Tran, Miller, & Kay 1992; Tran 1995a, 1995b, 1995c). Additional evidence in favor of the Seyfert unification theory comes from the apparent deficit of ionizing photons in many Seyfert 2 galaxies (see, e.g., Wilson, Haniff, & Ward 1988; Kinney et al. 1991; Storchi-Bergmann, Mulchaey, & Wilson 1992a) and the detection of extended anisotropic "ionization cones" around several of these objects (see, e.g., Unger et al. 1987; Pogge 1989; Tadhunter & Tsvetanov 1989; Evans et al. 1991; Storchi-Bergmann, Wilson, &

[1] Department of Astronomy, University of Maryland, College Park, MD 20742; veilleux@astro.umd.edu.

[2] Visiting Astronomer at the United Kingdom Infrared Telescope, which is operated by the Royal Observatory Edinburgh on behalf of the U.K. Science and Engineering Research Council.

[3] The W. M. Keck Observatory, 65-1120 Mamalahoa Highway, Kamuela, HI 96743; rgoodrich@keck.hawaii.edu.

[4] McDonald Observatory, University of Texas at Austin, Austin, TX 78712; hill@astro.as.utexas.edu.

Baldwin 1992b; Wilson et al. 1993; Pogge & De Robertis 1993; Wilson & Tsvetanov 1994, and references therein). While these results argue for anisotropic continuum emission in Seyfert galaxies and are consistent with the idea of aspect-dependent obscuration, they do not show that a BLR exists in Seyfert 2's; therefore, these results do not demonstrate that all Seyfert galaxies are fundamentally the same.

Recent advances in infrared detector technology have produced an efficient new tool in the study of AGNs: infrared spectroscopy. In contrast to spectropolarimetry, which relies on the presence of a scattering region with large enough covering factor and optical depth to provide an indirect view of the deep interiors of AGNs, infrared spectroscopy can potentially penetrate the obscuring material and allow us to see the BLRs directly. This technique has proved very useful in the study of highly reddened BLRs in intermediate Seyfert galaxies (1.8's and 1.9's; Goodrich 1990; Rix et al. 1990) and has also had success finding obscured BLRs in some optically classified Seyfert 2 galaxies (see, e.g., Blanco, Ward, & Wright 1990; Hines 1991; Nakajima, Carleton, & Nishida 1991; Goodrich, Veilleux, & Hill 1994; Ruiz, Rieke, & Schmidt 1994). In Goodrich, Veilleux, & Hill (1994, hereafter Paper I), high-resolution ($R = 1260$) and low-resolution ($R = 345$ and 425) J-band spectra of 15 Seyfert 2 galaxies were analyzed. The presence of broad Paβ λ1.2818 emission was confirmed in three of these objects (MCG $-$05-23-16 and Mrk 463E [Blanco et al. 1990] as well as NGC 2992 [Rix et al. 1990]), while two others were considered possible candidates (Mrk 176 and NGC 5728). The high resolution and high signal-to-noise ratio (S/N) of these data allowed us to remove the narrow-line flux from the total line flux accurately and unambiguously and hence to get a better idea of the reddening affecting the BLR.

Given the relatively modest gain in optical depth by going from Hα to Paβ (a factor of only 3), the detection of as many as three obscured BLRs out of 15 objects is rather encouraging. Indeed, Paβ only probes the very edge ("skin") of the obscuring mass distribution, where extinctions are $A_V \lesssim 11$ (see Paper I for a discussion of this calculation), whereas Brγ λ2.1655 can probe to $A_V \approx 26$, and Brα λ4.0512 to $A_V \approx 68$. Notwithstanding the steeply rising 1–10 μm continua of Seyfert galaxies and the increased thermal background radiation at longer wavelengths, K-band and L-band observations should therefore allow us to extend the reach of our probe significantly. The present paper reports the results of such an attempt. High-resolution K-band spectra centered on Brγ were acquired for 10 of the 15 galaxies included in Paper I (hereafter called the Spring Sample). L-band spectra centered on Brα were also obtained for two of these objects (NGC 4388 and NGC 5506). Similar J-band and K-band data were obtained for an additional set of 17 Seyfert 2 galaxies (Fall Sample) to improve the statistical significance of our results.

The present paper is organized as follows. First, the techniques used to acquire and reduce our data are described in § 2. In § 3, the results of the new survey are presented and combined with those in Paper I to draw some general conclusions. The interpretation of these data is carried out in § 4. The implications of our results for the Seyfert unification theory are discussed in that section. The last part of § 4 focuses on the much debated origin of the strong line emission from [Fe II] and H_2. The conclusions from our study are summarized in § 5, along with a discussion of potentially rewarding avenues of research. The emission-line properties of each object are discussed in the Appendix, with particular emphasis on the presence or absence of broad components in the profiles of the infrared hydrogen recombination lines. We assume $H_0 = 75$ km s^{-1} Mpc^{-1} and $q_0 = 0.5$ throughout this paper.

2. OBSERVATIONS AND DATA ANALYSIS

All of the new data presented in this paper were taken with CGS4 on UKIRT (Mountain et al. 1990). A summary of the observations is presented in Table 1. The procedure used to obtain these data is detailed in Paper I. The 58 × 62 pixel Santa Barbara Research Corporation detector was stepped 6 times along the spectrum by steps of $\frac{1}{3}$ pixel to sample the data effectively and also to minimize the loss of data from bad pixels. The spectra acquired in 1993 December and 1994 March/April were obtained with a 3″ (1 pixel) slit, a grating with 150 lines mm^{-1}, and the short focal length (150 mm, SFL) camera. This setup results in a spectral resolution of about 1200 (i.e., 250 km s^{-1} in terms of velocity resolution) in the J band, 1400 (i.e., 215 km s^{-1}) at K, and 1030 (i.e., 290 km s^{-1}) at L. In 1994 September, we used a 1.″5 (1 pixel) slit, a grating with 75 lines mm^{-1}, and the long focal length (300 mm, LFL) camera. The resolution of these K-band spectra is about 670, or 450 km s^{-1}. All of the data were taken in sets of four observations ("quads") in which the object was moved back and forth between two points along the slit 10 pixels apart (equivalent to 30.″8 with the SFL camera and 15.″4 with the LFL camera).

Preliminary data reduction was done on Mauna Kea using the standard UKIRT software. This includes bias subtraction, flat-fielding, and interpolation across known bad pixels. Subsequent reduction was done using VISTA, a data reduction package developed at Lick Observatory. Following the same procedure as in Paper I, each quad was reduced by subtracting the two observations of the object at one slit position from the pair at the other slit position. This effectively removed the sky, and no other sky subtraction was found necessary. The seeing was generally much less than 1 pixel, and therefore typically more than 75% of the light of point sources was contained within a single row of the detector. Since we are interested only in the central, unresolved nucleus of Seyfert 2 galaxies, only the central row of data was extracted. Mrk 1210 was the only exception to this rule; owing to centering errors, the J-band spectrum of this galaxy was spread out over 2 pixels (see § A29). The internal photometric stability of the data, determined by intercomparing each set of quads for a given object, was found to be in most cases better than 25%. After removing the ion hits, the intensity of each individual spectrum was scaled to the brightest spectrum in the set and then averaged together. This procedure should in principle improve the photometric accuracy of our data. The "sawtooth" pattern due to differential slit losses between "subobservations" taken at different detector steps was removed using a VISTA procedure described in Paper I. The amplitude of this pattern was found to be 3%–5% for the bright atmospheric and flux standards and typically less than 1% for the galaxies.

Next, the data were wavelength calibrated using lamps of argon and krypton and the OH sky lines in the galaxy spectra. The OH line list of Osterbrock & Martel (1992) adapted to interstellar (vacuum) conditions was used for

TABLE 1

LOG OF OBSERVATIONS: SPRING AND FALL SAMPLES

Number	Object	Other Name	Date	Spectral Region	Exposure (minutes)	Resolution ($\lambda/\Delta\lambda$)	Spectral Aperture (arcsec)[a]
			The Spring Sample				
1	MCG −05-23-16	A0945–30	1992 Apr 11	J	56	1260	3.0 × 3.0
			1994 Apr 1	K	56	1400	3.0 × 3.0
2	Mrk 3	...	1992 Mar 18	J	32	345	3.0 × 3.0
			1992 Mar 19	J	88	345	3.0 × 3.0
3	Mrk 78	...	1992 Mar 21	J	120	345	3.0 × 3.0
4	Mrk 176	...	1992 Apr 11	J	24	1260	3.0 × 3.0
			1994 Apr 1	K	24	1400	3.0 × 3.0
5	Mrk 266SW	NGC 5256SW	1992 Apr 11	J	48	1260	3.0 × 3.0
			1994 Apr 1	K	64	1400	3.0 × 3.0
6	Mrk 266NE	NGC 5256NE	1992 Apr 11	J	48	1260	3.0 × 3.0
7	Mrk 463E	...	1992 Apr 9	J	32	345	3.0 × 3.0
			1992 Apr 10	J	120	1260	3.0 × 3.0
			1994 Mar 31	K	32	1400	3.0 × 3.0
8	Mrk 477	I Zw 92	1992 Apr 9	J	40	345	3.0 × 3.0
			1994 Apr 1	K	48	1400	3.0 × 3.0
9	Mrk 1388	...	1992 Apr 11	J	96	1260	3.0 × 3.0
10	NGC 2992	MCG −02-25-14	1992 Apr 10	J	60	1260	3.0 × 3.0
		Arp 245	1994 Mar 30	K	80	1400	3.0 × 3.0
11	NGC 3081	IC 2529	1992 Apr 9	J	60	345	3.0 × 3.0
12	NGC 4388	...	1992 Apr 10	J	60	1260	3.0 × 3.0
			1994 Mar 30	K	40	1400	3.0 × 3.0
			1994 Mar 30	L	66	1030	3.0 × 3.0
13	NGC 5252	...	1992 Apr 9	J	64	345	3.0 × 3.0
			1994 Apr 1	K	48	1400	3.0 × 3.0
14	NGC 5506	...	1992 Apr 10	J	32	1260	3.0 × 3.0
			1994 Mar 31	K	32	1400	3.0 × 3.0
			1994 Mar 30	L	72	1030	3.0 × 3.0
15	NGC 5728	MCG −03-37-5	1994 Mar 31	K	24	1400	3.0 × 3.0
			The Fall Sample				
16	Akn 79	...	1994 Sep 18	K	46	670	1.5 × 1.5
			1994 Sep 19	K	16	670	1.5 × 1.5
17	ESO 428-G14	M4-1/MCG −05-18-2	1993 Dec 3	J	36	1200	3.0 × 3.0
18	IC 5135	NGC 7130	1994 Sep 17	K	32	670	1.5 × 1.5
19	Mrk 1	NGC 449	1994 Sep 18	K	40	670	1.5 × 1.5
			1994 Sep 19	K	8	670	1.5 × 1.5
20	Mrk 348	NGC 262	1993 Dec 5	J	72	1200	3.0 × 3.0
			1994 Sep 17	K	64	670	1.5 × 1.5
21	Mrk 403	...	1993 Dec 4	J	30	1200	3.0 × 3.0
22	Mrk 533	NGC 7674	1993 Dec 5	J	48	1200	3.0 × 3.0
		Arp182	1994 Sep 18	K	40	670	1.5 × 1.5
			1994 Sep 19	K	8	670	1.5 × 1.5
23	Mrk 573	UM 363	1993 Dec 5	J	60	1200	3.0 × 3.0
			1994 Sep 17	K	56	670	1.5 × 1.5
24	Mrk 622	...	1993 Dec 4	J	48	1200	3.0 × 3.0
25	Mrk 917	MCG+05-53-09	1994 Sep 18	K	32	670	1.5 × 1.5
			1994 Sep 19	K	8	670	1.5 × 1.5
26	Mrk 1066	...	1993 Dec 5	J	24	1200	3.0 × 3.0
			1994 Sep 17	K	16	670	1.5 × 1.5
27	Mrk 1073	MCG+7-7-37	1993 Dec 5	J	30	1200	3.0 × 3.0
			1994 Sep 18	K	40	670	1.5 × 1.5
			1994 Sep 19	K	24	670	1.5 × 1.5
28	Mrk 1157	NGC 591	1994 Sep 18	K	32	670	1.5 × 1.5
			1994 Sep 19	K	8	670	1.5 × 1.5
29	Mrk 1210	...	1993 Dec 3	J	72	1200	6.0 × 3.0
			1994 Mar 31	K	80	1400	3.0 × 3.0
30	NGC 1068	M 77	1994 Sep 17	K	8	670	1.5 × 1.5
31	NGC 2110	MCG −01-15-4	1993 Dec 3	J	36	1200	3.0 × 3.0
			1993 Dec 5	J	24	1200	3.0 × 3.0
			1994 Sep 17	K	32	670	1.5 × 1.5
32	NGC 7172	...	1994 Sep 17	K	16	670	1.5 × 1.5
33	NGC 7212	...	1994 Sep 18	K	36	670	1.5 × 1.5
			1994 Sep 19	K	16	670	1.5 × 1.5

[a] This column lists the size of the spectral aperture, i.e. the width of the slit × the width of the spectrum that was extracted for the analysis.

this purpose. The atmospheric absorption features were removed from the spectra of the galaxies using observations of nearby early-type (B and A) and late-type (G, K, or M) stars. Finally, the galaxy spectra were put on an absolute flux scale using observations of flux standards from Elias et al. (1982). The absolute zero points used in this procedure were those of Neugebauer et al. (1979). An attempt was also made in some cases to remove the underlying stellar features in the galaxy spectrum by subtracting off the spectrum of a "galaxy template" obtained on the same run. The spectra of the early-type galaxies NGC 1700 and NGC 3379 were used for this purpose.

The intensities of the emission lines in the reduced spectra were determined using GAUSS, an interactive VISTA program that removes the underlying continuum from the data and fits analytic line profiles. In most cases, the line profiles chosen were Gaussians. In a few cases, however, a linear combination of a Gaussian and a Lorentzian of the same FWHM and peak strength was found to fit the line profiles significantly better (see Appendix).

3. GENERAL RESULTS

The spectra obtained in the course of the new survey are presented in Figures 1 and 2. The new *K*- and *L*-band observations of the objects in the Spring Sample are presented in Figure 1; these objects were all part of our previous *J*-band survey (Paper I; the *J*-band spectra of these objects are not shown in Fig. 1). Figure 2 presents the full set of spectra on the objects in the Fall Sample. Table 3 lists the fluxes and line widths of the emission lines detected in these spectra. Also listed in this table are the spectral parameters derived in Paper I, the intensities and line widths of Hα and Hβ taken from the literature, and the color excesses, $E(B-V)$, determined from the optical and infrared emission-line flux ratios (discussed in more detail below). No attempt was made to measure the strength of the absorption features in our spectra. Our spectra do not extend longward enough to include the CO first-overtone feature at 2.3 μm. The metal lines often observed in galaxies (see, e.g., Goldader et al. 1995; Hawarden et al. 1995) are weak in most of our objects. Emission from hot (500–2000 K) dust or from a power-law nonthermal continuum is the likely cause for the weak equivalent widths of these features.

The *J*-band spectra of our sample galaxies are often characterized by strong emission from Paβ and [Fe II] λ1.2567. The [Fe II]/Paβ ratios in our galaxies cover a broad range from less than 1/3 to more than 5, with most of the objects having F([Fe II]) $\approx F$(Paβ). The widths of the [Fe II] profiles are significantly different from those of Paβ, which indicates that the [Fe II] emission is produced in a different volume of gas than the Paβ emission. The origin of the [Fe II] emission in Seyfert galaxies will be discussed in detail in § 4.2 below. The other feature present at 1.27114 μm in most of our spectra is [S III] λ0.95321 from the grating's fourth-order spectrum (see Paper I). The intensity of this feature is inaccurate and has not been tabulated in Table 3. The only other emission line detected with any certainty in the *J*-band spectra of our Seyfert galaxies is He I λ1.27887. This feature often lies on the blue wing of Paβ and therefore complicates the search for broad Paβ.

The *K*-band spectra of our sample galaxies are generally dominated by strong Brγ and H_2 1–0 $S(1)$ λ2.121 emission. The intensity of H_2 λ2.121 relative to Brγ varies from $\sim\frac{1}{2}$ to 4. Weaker emission from H_2 1–0 $S(0)$ λ2.223 is also visible in some galaxies. As in the case of [Fe II], the widths of the H_2 emission-line profiles are often significantly different from those of Brγ, but they present no clear tendency to be systematically narrower or broader than that of Brγ. The H_2 λ2.121 luminosities in our sample galaxies range from 3×10^{38} ergs s^{-1} to 3×10^{40} ergs s^{-1}. These luminosities translate into hot H_2 masses of order 100–10,000 $M_\odot$ if the hot H_2 molecules are thermalized at $T = 2000$ K (Scoville et al. 1982). The excitation processes responsible for the H_2 emission in our Seyfert galaxies will be discussed in § 4.3.

Weaker emission from He I λ2.058 is also visible in some galaxies. This emission line is produced through the transition of He I singlets from 2 ^1P to 2 ^1S. As a consequence, the strength of the He I λ2.058 emission in Seyfert 2 galaxies is less affected by complex radiative transfer effects than the other strong infrared He I line at 1.0830 μm (see, e.g., Osterbrock 1989; Rudy et al. 1989). The He I λ2.058/Brγ ratio basically reflects the relative importance of UV photons with energy greater than 24.6 and 13.6 eV (the ionization potentials of helium and hydrogen, respectively). This ratio therefore has a strong dependence on the spectral shape of the ionizing radiation. The He I λ2.058/Brγ ratio was measured in nine of our sample galaxies; values range from 0.16 to 0.61 with an average of 0.35. From equation (5) of Doyon, Puxley, & Joseph (1992), these values of He I λ2.058/Brγ imply that the production rate of ionizing photons with energies above 24.6 eV represents 3%–10% of the total ionization rate. This result suggests a steeper spectral energy distribution than generally assumed in Seyfert 2 galaxies (e.g., Ferland & Osterbrock 1986 derived $\alpha \approx 1.4$, implying a relative proportion of ionizing photons with energies between 24.6 and 1,000 eV above 50%). This conclusion should be treated with caution since the He I λ2.058/Brγ ratio is not simply a function of the hardness of the ionizing radiation field but also depends on the detailed geometry of the ionized gas, its density, the dust content, the velocity structure, and helium abundance (Shields 1993).

Listed in columns (12), (13), and (14) of Table 3 are the reddenings to the *narrow*-line regions determined from the Hα_n/Hβ_n, Paβ_n/Hα_n, and Brγ_n/Hα_n ratios and assuming the intrinsic ratios and interstellar extinction coefficients listed in Table 2. Disagreement between the various $E(B-V)$ for a given object may have a number of causes. First, the intrinsic line ratios may differ from those adopted. Here, we

TABLE 2

INTRINSIC FLUX RATIOS AND EXTINCTION COEFFICIENTS

Line (1)	λ(μm) (2)	$F/F_{H\beta}$ (3)	$A_\lambda/E(B-V)$ (4)
Hβ	0.4861	1.00	3.615
Hα.....	0.6563	3.10	2.45
Paγ	1.0938	0.090	1.100
Paβ.....	1.2818	0.162	0.83
Paα.....	1.8751	0.332	0.44
Brγ	2.1655	0.0275	0.35
Brα	4.0512	0.0779	0.134

NOTE.—Col. (1): Line identification. Col. (2): Wavelength. Col. (3): Intrinsic flux ratio relative to Hβ assuming Case B recombination with $T = 10^4$ K and $N_e = 10^4$ cm^{-3} (Osterbrock 1989). The Hα/Hβ ratio takes into account collisional effects (see § 3). Col. (4): Extinction coefficient from Whitford 1958 and Rieke & Lebofsky 1985.

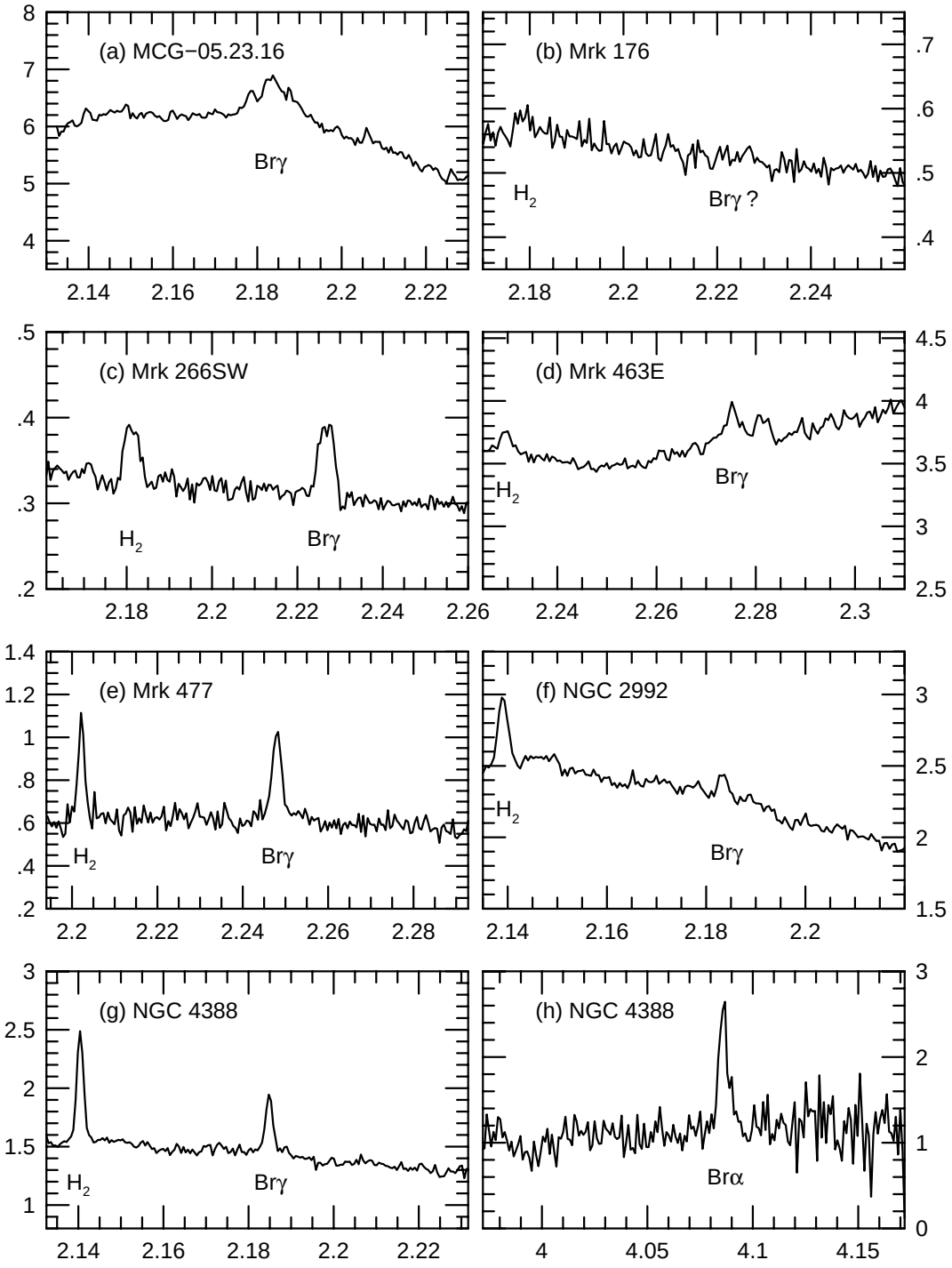

FIG. 1.—Reduced K- and L-band spectra of the Spring Sample—f_λ is plotted vs. $\lambda_{\rm observed}$. The units of the vertical axis are 10^{-11} ergs s^{-1} cm^{-2} μm^{-1}, while the wavelength scale is in μm.

assumed Case B recombination for all the line ratios with the exception of $H\alpha_n/H\beta_n$, where possible collisional effects were taken into account (Table 2; Ferland & Netzer 1983; Halpern & Steiner 1983; Gaskell 1984; Gaskell & Ferland 1984; Binette et al. 1990). Second, dust scattering may be important if the dust is mixed in with the narrow line gas. This effect will preferentially enhance $H\beta$ relative to the lines at longer wavelengths. The values of the reddening listed in Table 3 are strictly valid only if dust acts as a discrete absorbing screen in front of the line-emitting region. Third, absorption features from the underlying stellar continuum may affect the emission-line spectrum of some objects. Fourth, differential slit loss, seeing, centering errors, and guiding effects may affect the $Pa\beta_n/H\alpha_n$ and $Br\gamma_n/H\alpha_n$ ratios. This is particularly relevant in objects that are nearby and are known to have extended NLRs. If any of these objects were observed through the smaller $1''.5 \times 1''.5$ aperture, the flux of $Br\gamma_n$ may be underestimated relative to that of $H\alpha_n$, which results in an underestimate of the reddening derived from $Br\gamma_n/H\alpha_n$. This effect may explain the anomalously small $Br\gamma_n/H\alpha_n$ reddenings found in several Fall targets. Finally, discrepancies between the

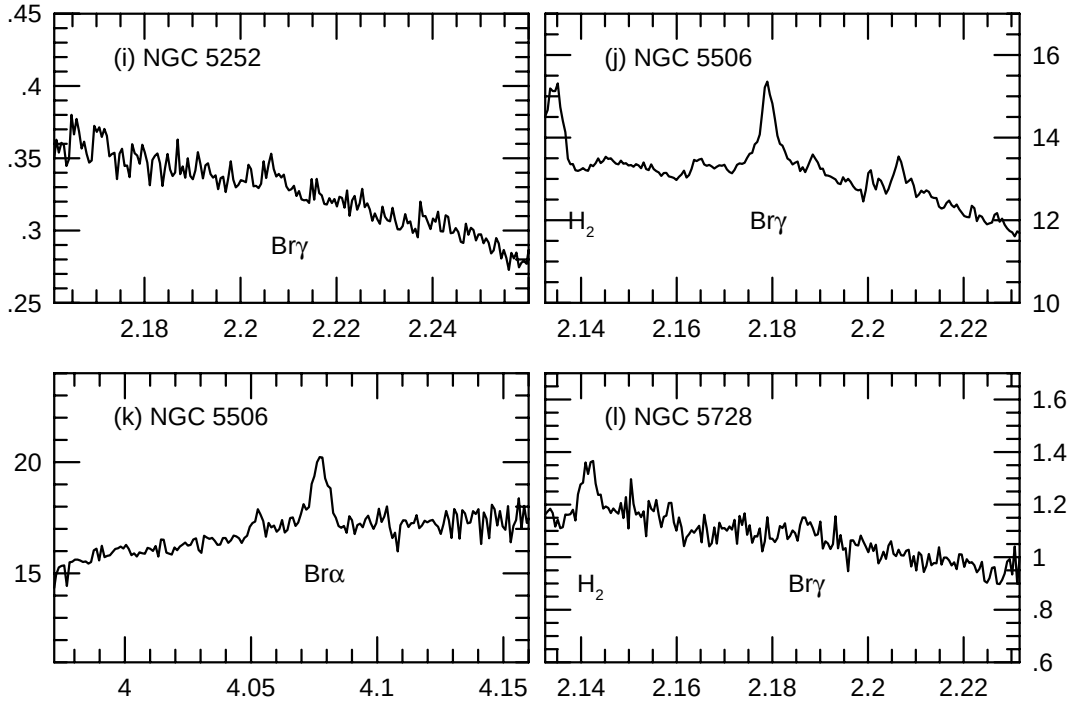

FIG. 1—*Continued*

various $E(B-V)$ may also reflect real differences in dust columns. The infrared lines may be produced in a highly reddened portion of the NLR that is simply not visible at optical wavelengths. This effect may explain the small amounts of reddening determined from $H\alpha_n/H\beta_n$ in Mrk 266NE, Mrk 533, NGC 3081, NGC 5506, and IC 5135.

4. DISCUSSION

4.1. *Implications for the Seyfert Unification Theory*

Among our sample of 33 optically classified Seyfert 2 galaxies, the presence of broad (FWHM $\approx$ 2000 km s^{-1}) infrared hydrogen recombination lines is confirmed in MCG −05-23-16, Mrk 463E, and NGC 2992. Broad-line emission may also be present in the Paβ profile of Mrk 176, Mrk 348, Mrk 1210, NGC 2110, and NGC 5728 and in the Brγ profile of Mrk 348, Mrk 477, Mrk 1210, and NGC 2110. The broad-line emission in these objects is interpreted as evidence for obscured high-density BLRs based on (1) the absence of broad wings in the profile of the forbidden [Fe II] λ1.257 and H_2 λ2.122 line or (2) the lack of observational evidence for powerful high-velocity ($\sim$2000 km s^{-1}) outflows in these objects (see references in § 4.3). In NGC 5506, however, we detected highly reddened wings that become more readily visible at longer wavelengths but found no evidence for a genuine high-density BLR.

Of the 33 objects studied here, at least eight have broad Balmer lines in polarized light (Mrk 3, Mrk 348, Mrk 463E, Mrk 477, Mrk 533, Mrk 1210, NGC 1068, and NGC 7212; Tran 1995a and references therein), while two other objects are considered potential candidates (Mrk 266SW and Mrk 573; Kay 1994). Combining the results from spectropolarimetry and infrared spectroscopy, perhaps as many as 40% of the Seyfert 2 galaxies in our sample harbor a BLR.

Spectropolarimetric studies indicate that hidden Seyfert 1 galaxies do not differ significantly from the "normal" Seyfert 1's (Miller & Goodrich 1990; Tran 1995a). It is therefore natural to ask whether the obscured broad-line regions detected through infrared spectroscopy also have properties that are similar to the BLRs detected in polarized light or the BLRs in normal Seyfert 1's. From Table 3, the widths of the broad components to Paβ and Brγ range from $\sim$1000 to 4500 km s^{-1} with an average value of approximately 2000 km s^{-1}. These line widths lie on the narrow end of the distribution for Seyfert 1 galaxies (see, e.g., Osterbrock 1977; Goodrich 1989). The infrared lines are also systematically narrower than the lines detected in polarized light. Note, however, that the sensitivity of our observations to very broad ($\gtrsim$5000 km s^{-1}) emission features is rather poor owing to the fairly high spectral resolution of our spectra and the presence of several stellar absorption features that complicate the interpretation of the data. Nevertheless, the broad component detected at Paβ or Brγ in these objects often is an order of magnitude stronger than the value expected from the scattered flux assuming Case B recombination (see Appendix). Only a small fraction ($\lesssim$10%) of the total broad-line flux is therefore seen in scattered light.

It is also interesting to compare the dereddened broad-line luminosities of the obscured BLRs with those of normal Seyfert 1's. Unfortunately, firm estimates of the broad-line extinction exist for very few objects in our sample. This exercise was carried out only for MCG −05-23-16, NGC 2110, and NGC 2992. In NGC 2992, we used the visual extinction derived from the J-band and K-band spectra [$A_V(J) \approx A_V(K) \approx 8$; see Table 5], while the BLR extinctions of MCG −05-23-16 and NGC 2110 were estimated from the X-ray column depths (see Table 5 and discussion of the caveats below). Using the broad-line Paβ fluxes and the extinction coefficients of Table 2, $L(H\beta_b)_0 \approx 4 \times 10^{43}$ ergs s^{-1}, $< 6 \times 10^{41}$ ergs s^{-1}, and 3×10^{41} ergs s^{-1} for MCG −05-23-16, NGC 2110, and NGC 2992, respectively. These values are similar to the broad Hβ luminosities of normal Seyfert 1's (10^{41}–10^{43} ergs s^{-1}; Blumenthal, Keel, &

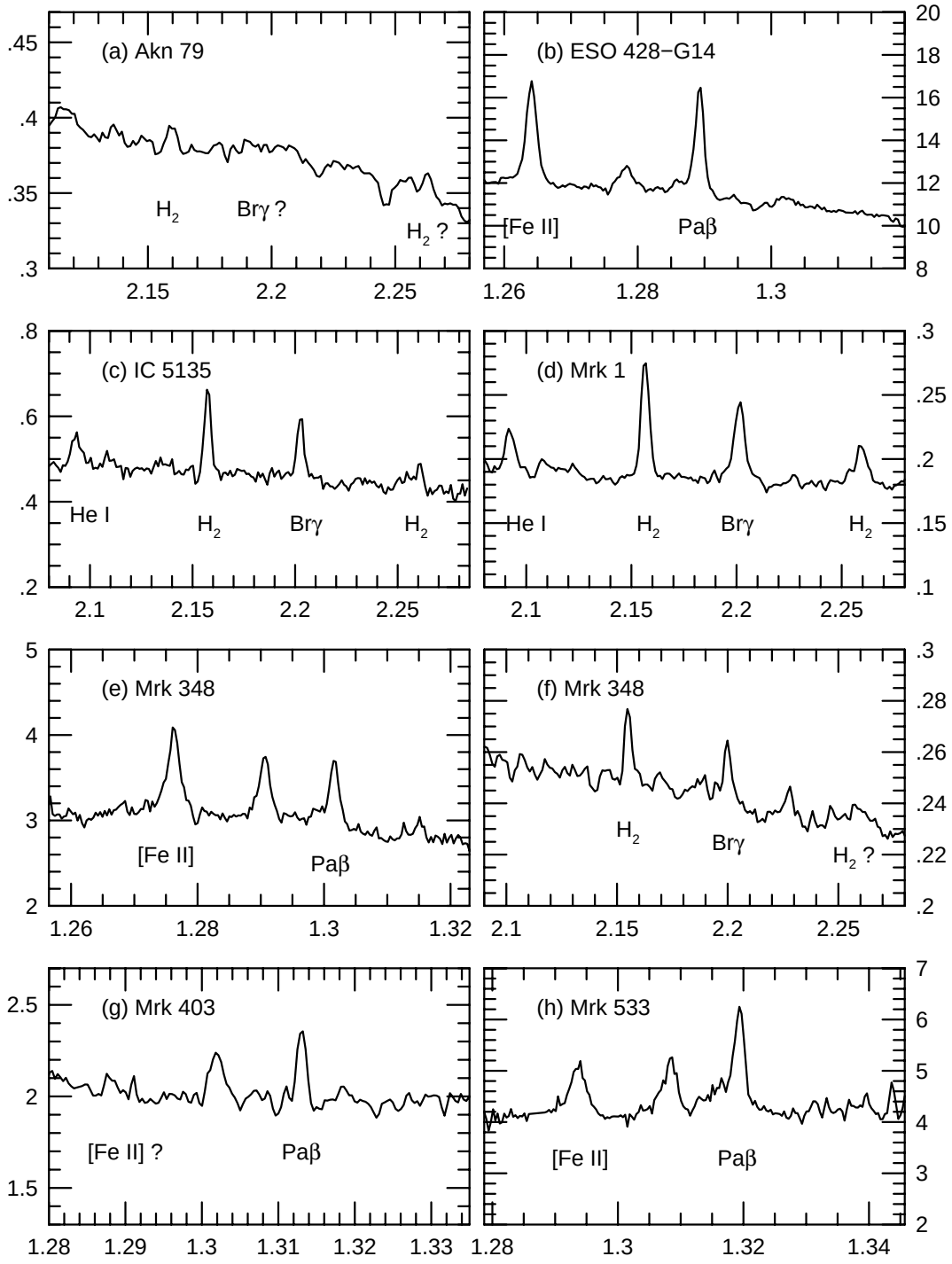

FIG. 2.—Reduced J- and K-band spectra of the Fall Sample—f_λ is plotted vs. $\lambda_{\rm observed}$. The units of the vertical axis are 10^{-11} ergs s^{-1} cm^{-2} μm^{-1}, while the wavelength scale is in μm.

Miller 1982). Moreover, the ratios of the hard X-ray flux to the dereddened broad Hα flux in MCG −05-23-16 ($\sim$2), NGC 2110 ($\lesssim$2), and NGC 2992 ($\sim$8) are typical of unreddened Seyfert 1 galaxies ($\sim$7; see, e.g., Ward et al. 1987).

These results are consistent with the idea that at least some Seyfert 2's are simply Seyfert 1's seen from an angle at which their central regions are obscured from our direct view by optically thick material. The obscuring mass distribution can take several forms: it may be geometrically thick like a torus (Krolik & Begelman 1986; Pier & Krolik 1992a) or like a sphere with evacuated biconical regions at the poles (Königl & Kartje 1994; Hill, Goodrich, & DePoy 1996), or it may be geometrically thin but strongly warped (Phinney 1989; Sanders et al. 1989). The infrared data can in principle help us distinguish between these various possibilities since the optical obscuration due to dust is not expected to be of the same magnitude and have the same dependence on polar angle for these models. In the radiation pressure–supported molecular torus model of Pier & Krolik (1992a), the visual extinction is expected to increase rapidly beyond θ_c, the opening angle of the torus, reaching values perhaps as large as $\sim$1000 mag when the torus is

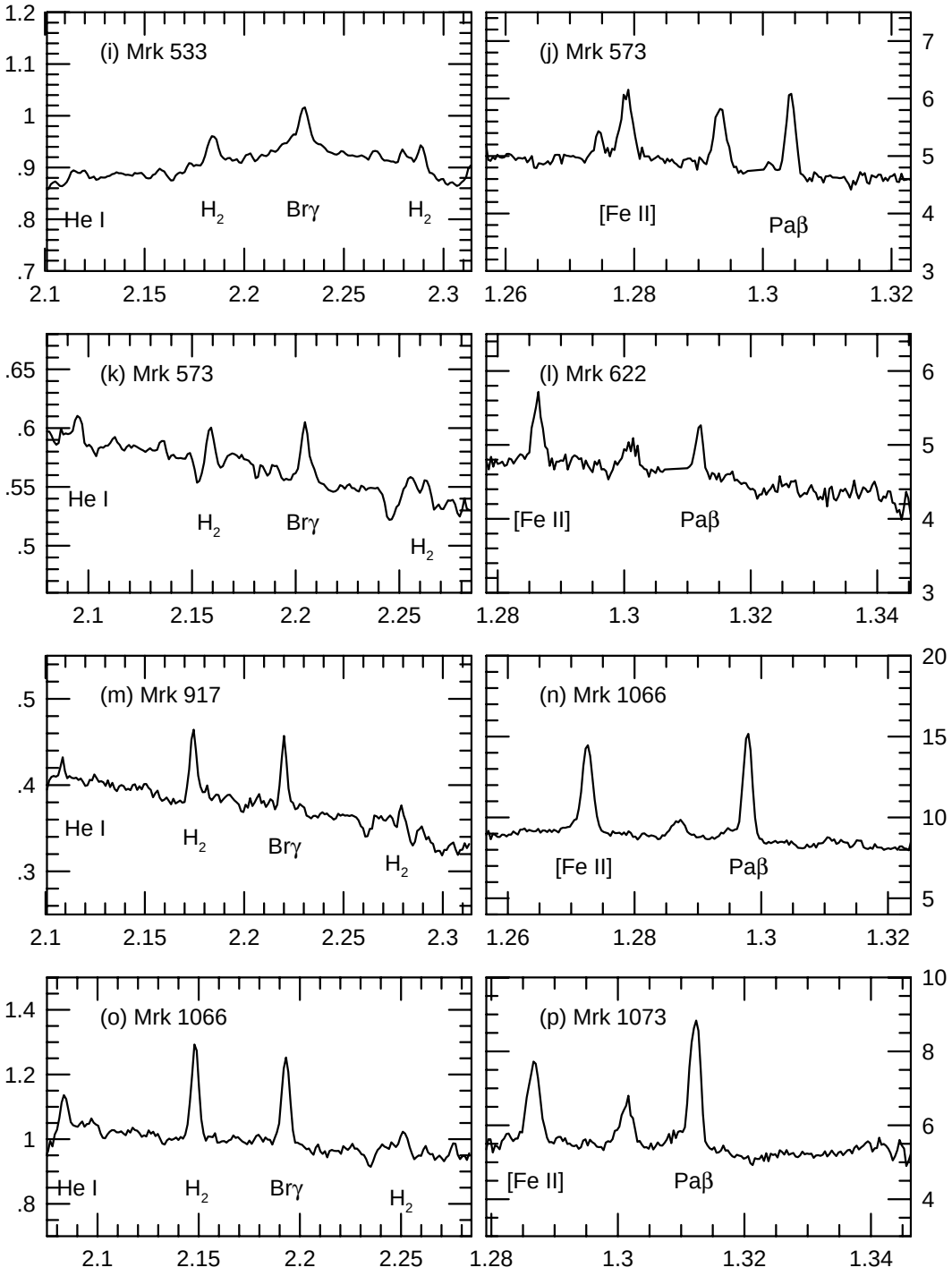

FIG. 2—*Continued*

viewed edge-on. A sharp increase in dust extinction is also predicted in the warped disk model when the line of sight starts intercepting the dusty disk, unless the distribution of the molecular gas in the disk is patchy. In this case, however, the thin geometry of the obscuring material is unlikely to produce visual extinction much larger than ~ 100 mag. The extinction profile in the wind model of Königl & Kartje (1994) depends somewhat on the importance of the magnetic flux relative to the mass flux and on the specific angular momentum. In the set of simulations that best reproduce the opening angle of the obscuring material in Seyfert galaxies, Königl & Kartje find that A_V is a relatively smooth function of the polar angle, increasing from 1 to 50 mag when the polar angle changes from $\sim 40°$ to 70° and that it never reaches values much larger than 100 mag except when the dusty wind is viewed nearly edge-on ($\theta > 80°$; see Fig. 5 of Königl & Kartje 1994).

Table 5 lists estimates of the visual extinctions toward the BLRs in our sample galaxies. In only one galaxy (NGC 2992) was it possible to derive reddenings directly from the measured strengths of broad Hα, Paβ, and Brγ. For galaxies with detected broad Paβ and/or Brγ but no obvious broad Hα, the intensity of broad Hα was assumed not to be more than one-fifth of the observed narrow Hα flux. The only

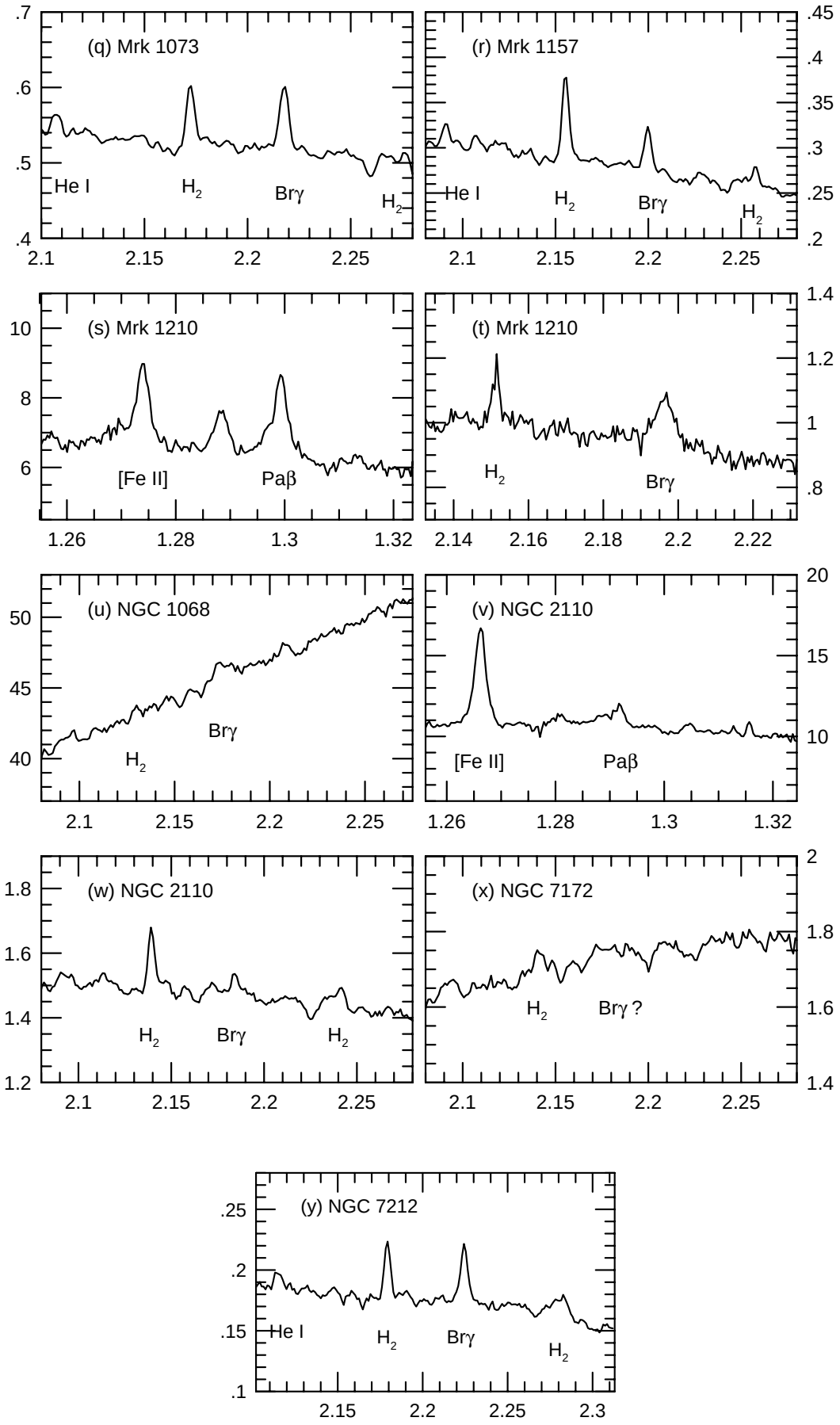

FIG. 2—*Continued*

TABLE 3

OPTICAL AND INFRARED LINE MEASUREMENTS

OBJECT (1)	$H\beta_n$ (2)	$H\alpha_n$ (3)	$Pa\beta_n$ (4)	$Pa\beta_b$ (5)	[Fe II] 1.257 (6)	He I 2.058 (7)	H_2 2.122 (8)	H_2 2.223 (9)	$Br\gamma_n$ (10)	$Br\gamma_b$ (11)	$E(B-V)_n$ $H\alpha/H\beta$ (12)	$E(B-V)_n$ $Pa\beta/H\alpha$ (13)	$E(B-V)_n$ $Br\gamma/H\alpha$ (14)	NOTES (15)
The Spring Sample														
MCG–05-23-16.....	1.25[a]	10.0[a]	1.98	31.3	1.22	...	...	...	...	6.91	0.88	0.89	<2.25	1
	...	...	<100	2490	344	...	...	...	...	1485				
	...	210[b]	0	2478	246	...	...	...	...	1469				
Mrk 3	30[c]	200[c]	11.5	...	16.4	...	...	...	...	...	0.71	0.06	...	
	...	...	...	...	...	...	...	...	...	...				
	819[d]	966[d]	...	...	...	...	...	...	...	...				
Mrk 78	1.4[c]	9.1[c]	1.37	...	1.96	...	...	...	...	...	0.69	0.71	...	
	...	...	...	...	...	...	...	...	...	...				
	...	1075[e]	...	...	...	...	...	...	...	...				
Mrk 176.....	0.67[c]	4.4[c]	0.38	...	1.65	...	0.220	...	0.056::	...	0.70	0.34	0.19::	
	...	...	519	...	638	...	440	...	...	...				
	...	451[f]	460	...	591	...	384	...	...	...				
Mrk 266SW	3.33[g]	14.8[g]	5.51	...	2.61	...	0.278	...	0.367	...	0.34	1.32	0.53	
	...	...	459	...	402	...	530	...	587	...				
	...	390[h]	391	...	322	...	484	...	546	...				
Mrk 266NE.....	1.18[g]	6.76[g]	4.01	...	5.09	...	...	...	...	...	0.57	1.63	...	
	...	...	328	...	496	...	...	...	...	...				
	...	315[h]	224	...	434	...	...	...	...	...				
Mrk 463E	3.4[c]	19[c]	3.01	24.5	2.04	...	0.521	...	0.272	1.4::	0.55	0.74	0.25	
	...	...	300	1810	300	...	382	...	181	1090::			(1.20)	
	...	586[f]	180	1794	180	...	316	...	0	1070::				
Mrk 477.....	15[c]	81[c]	10.4	...	7.76	...	0.912	...	0.953	$\lesssim$0.76::	0.52	0.60	0.15	
	...	...	...	...	...	...	241	...	315	1640::			(<0.45)	
	...	365[i]	...	...	...	...	109	...	230	1630::				
Mrk 1388	2.5[c]	13[c]	1.95	...	0.78	...	...	...	...	...	0.48	0.71	...	
	...	...	284	...	458	...	...	...	...	...				
	...	320[j]	152	...	390	...	...	...	...	...				
NGC 2992	3.3[c]	23	2.92	5.00	8.62	...	1.2:	...	0.306	$\lesssim$2.1::	0.76	0.60	0.21	2, 3
	...	...	200	...	400	...	330	...	259	4422::			(<1.28)	3
	...	201[f]	0	...	320	...	250	...	144	4417::				3
NGC 3081	2.9[c]	13[c]	5.46	...	3.13	...	...	...	...	...	0.34	1.40	...	
	...	...	...	...	...	...	...	...	...	...				
	...	164[f]	...	...	...	...	...	...	...	...				
NGC 4388	5.2[c]	30[c]	8.09	...	7.37	...	1.86	...	1.13	...	0.58	1.10	0.75	
	...	...	250	...	500	...	257	...	292	...				
	144[d]	213[d]	70	...	439	...	141	...	198	...				
NGC 5252	3.7[k]	...	1.68	...	3.08	...	...	...	0.066	...	...	0.40::	−0.14::	4
	...	...	...	...	...	...	...	...	473	...				
	...	510[e]	...	...	...	...	...	...	421	...				
NGC 5506	4.4[c]	33[c]	85.1	...	28.5	...	...	...	11.8	...	0.82	2.61	1.91	
	...	...	652	...	450	...	...	...	650	...				
	342[d]	329[d]	606	...	381	...	...	...	614	...				
NGC 5728	5.8[c]	34[c]	2.18	...	2.99	...	0.701	...	0.222	...	0.59	0.14	−0.16	
	...	...	...	...	...	...	502	...	345	...				
	...	260[l]	...	...	...	...	454	...	270	...				

TABLE 3—*Continued*

Object (1)	$H\beta_n$ (2)	$H\alpha_n$ (3)	$Pa\beta_n$ (4)	$Pa\beta_b$ (5)	[Fe II] 1.257 (6)	He I 2.058 (7)	H_2 2.122 (8)	H_2 2.223 (9)	$Br\gamma_n$ (10)	$Br\gamma_b$ (11)	$E(B-V)_n$ $H\alpha/H\beta$ (12)	$E(B-V)_n$ $Pa\beta/H\alpha$ (13)	$E(B-V)_n$ $Br\gamma/H\alpha$ (14)	Notes (15)
The Fall Sample														
Akn 79	0.38[c]	3.17[c]	...	...	...	...	0.053:	...	<0.1::	...	0.92	...	<0.66::	
	...	...	...	...	...	...	540:	...	...	...				
	...	355[e]	...	...	...	...	298:	...	...	...				
ESO 428-614.....	20[m]	93[m]	8.26	...	9.16	...	...	...	...	...	0.38	0.36	...	5
	...	...	363	...	453	...	...	...	...	...				5
	...	650[m]	263	...	378	...	...	...	...	...				5
IC 5135.....	1.6[n]	8.9[n]	...	...	...	0.387	0.796	0.211	0.635	...	0.54	...	1.08	
	...	...	...	...	...	770	503	468	552	...				
	...	450[e]	...	...	...	625	225	129	320	...				
Mrk 1	2.87[c]	16.8[c]	...	...	...	0.165	0.455	0.192	0.411	...	0.59	...	0.52	
	...	...	...	...	...	724	641	896	882	...				
	...	520[e]	...	...	...	567	456	775	759	...				
Mrk 348	1.64[c]	9.61[c]	1.36	...	2.38	...	0.116	0.064:	0.087	...	0.59	0.67	0.01	6
	...	...	395	...	586	...	506	1260:	511	...				6
	...	365[e]	306	...	530	...	231	1177:	242	...				6
Mrk 403	0.62[c]	3.54[c]	0.599	...	<0.203	...	...	...	...	...	0.57	0.79	...	
	...	...	305	...	422	...	...	...	...	...				
	...	...	175	...	340	...	...	...	...	...				
Mrk 533	3.82[c]	18.6[c]	6.58	...	3.67	0.173	0.336	0.14:	1.04	...	0.42	1.28	0.95	
	...	...	624	...	848	1151	804	441:	1424	...				
	...	323[d]	572	...	810	1059	666	000:	1351	...				
Mrk 573	4.96[c]	21.3[c]	2.61	...	2.44	0.078	0.127	<0.11:	0.260	...	0.30	0.57	0.17	7
	...	...	383	...	490	525	502	754:	712	...				7
	...	190[e]	290	...	421	270	222	605:	552	...				7
Mrk 622	0.29[c]	5.32[c]	1.02	...	1.53	...	...	...	...	...	1.66	0.87	...	
	...	...	325	...	401	...	...	...	...	...				
	...	350[e]	208	...	314	...	...	...	...	...				
Mrk 917	1.31[c]	13.0[c]	...	...	...	0.048	0.350	0.078:	0.294	...	1.08	...	0.48	
	...	...	...	...	...	277	568	368:	462	...				
	...	...	...	...	...	000	347	000:	105	...				
Mrk 1066	4.28[c]	37.1[c]	11.5	...	11.3	0.429	1.36	0.47:	1.35	...	0.96	1.19	0.73	8
	...	...	371	...	467	551	601	1118:	641	...				8
	280[d]	279[d]	274	...	394	318	398	1023:	456	...				8
Mrk 1073	3.26[c]	20.6[c]	7.25	...	5.20	0.120	0.391	0.049:	0.468	...	0.66	1.28	0.49	9
	...	...	433	...	527	689	625	411	695:	...				9
	197[d]	...	354	...	464	522	434	000	530:	...				9
Mrk 1157	1.96[c]	11.5[c]	...	...	...	0.066	0.428	0.094	0.235	...	0.59	...	0.43	
	...	...	...	...	...	480	599	556	616	...				
	217[d]	225[d]	...	...	...	167	395	327	421	...				
Mrk 1210	9.12[o]	47.4[o]	3.74	<5.9:	7.71	...	0.409	...	0.711	<0.742	0.48	0.28	0.27	
	...	...	496	1644:	791	...	326	...	748	3062		(<0.91)	(<0.64)	
	...	...	428	1624:	750	...	245	...	711	3055				
NGC 1068	160[c]	715[c]	...	...	...	...	2.9::	...	12.7	...	0.34	...	0.36	
	...	...	...	...	...	...	496::	...	1448	...				
	1241[d]	...	...	...	...	...	209::	...	1376	...				
NGC 2110	2.74[c]	21.7[c]	≳1.77	≲3.15	15.0	...	0.734	0.40:	≳0.187	≲0.495	0.87	≳0.30	≳−0.01	
	...	...	393	1230	588	...	535	1206:	453	3159		(<0.98)	(<0.65)	
	...	420[d]	303	1204	532	...	289	1119:	052	3127				

TABLE 3—*Continued*

Object (1)	$H\beta_n$ (2)	$H\alpha_n$ (3)	$Pa\beta_n$ (4)	$Pa\beta_b$ (5)	[Fe II] 1.257 (6)	He I 2.058 (7)	H_2 2.122 (8)	H_2 2.223 (9)	$Br\gamma_n$ (10)	$Br\gamma_b$ (11)	$E(B-V)_n$ $H\alpha/H\beta$ (12)	$E(B-V)_n$ $Pa\beta/H\alpha$ (13)	$E(B-V)_n$ $Br\gamma/H\alpha$ (14)	Notes (15)
NGC 7172.....	...	...	...	...	$\lesssim 0.8$[p]	...	<0.241	<0.160	<0.427	...	$\gtrsim 0.8$[q]	...	...	
	...	...	...	...	...	...	644	1655:	2910::	...				
	...	245[q]	...	...	...	...	461	1593:	2875::	...				
NGC 7212.....	4.39[e]	22.2[e]	...	...	...	0.064	0.201	<0.15:	0.278	...	0.46	...	0.18	
	...	...	...	...	...	673	557	1405:	758	...				
	...	435[e]	...	...	...	500	328	1331:	610	...				

Note.—For each emission line of each object, we list the observed line flux in 10^{-14} ergs s^{-1} cm^{-2} on the first row, the observed line width in km s^{-1} on the second row, and the line width corrected for the instrumental resolution in km s^{-1} on the third row. Col. (1): Name of object. Cols. (2)–(11): Line fluxes and line widths for narrow $H\beta$, narrow $H\alpha$, narrow $Pa\beta$, [Fe II] λ1.257, He I λ2.058, H_2 λ2.122, H_2 λ2.223, narrow $Br\gamma$, and broad $Br\gamma$, respectively. Cols. (12)–(14): Narrow-line color excesses derived using

$$E(B-V)\left(\frac{\text{line 2}}{\text{line 1}}\right) = \frac{2.5}{[A_1/E(B-V)] + [A_2/E(B-V)]} \log\left[\frac{(F_2/F_1)}{(F_2/F_1)_0}\right]$$

with the intrinsic flux ratios and interstellar extinction coefficients listed in Table 2. The reddenings enclosed in parentheses were derived using the sum of the broad and narrow-line fluxes; they should therefore be considered upper limits to the actual values. Col. 15: Notes on individual galaxies.

Notes on Individual Galaxies.—(1) Durret & Bergeron 1988 argue for the presence in this galaxy of broad Hα with a flux of 18×10^{-14} ergs s^{-1} cm^{-2}. (2) Weak broad Hα may be present in this galaxy. Véron et al. 1980 measured $F(H\alpha_b) = 1.95 \times 10^{-14}$ ergs s^{-1} cm^{-2}, while Shuder 1980 measured $F(H\alpha_b) = 2.5 \times 10^{-13}$ ergs s^{-1} cm^{-2}. (3) The blue wing of [Fe II] in this galaxy may be contaminated by He I emission. (4) The color excesses are based on $Pa\beta_n/H\beta_n$ and $Br\gamma_n/H\beta_n$. (5) $Pa\beta$ is contaminated by He I λ1.27887 with a flux of 1.46×10^{-14} ergs s^{-1} cm^{-2} and a FWHM of 727 km s^{-1} after correction for the finite spectral resolution. (6) $Pa\beta$ is contaminated by He I λ1.27887 with a flux of 0.326×10^{-14} ergs s^{-1} cm^{-2} and a FWHM of 378 km s^{-1} after correction for the finite spectral resolution. (7) $Pa\beta$ is possibly contaminated by He I λ1.27887 with a flux of 0.453×10^{-14} ergs s^{-1} cm^{-2} and a FWHM of 413 km s^{-1} after correction for the finite spectral resolution. (8) $Pa\beta$ is contaminated by He I λ1.27887 with a flux of 1.98×10^{-14} ergs s^{-1} cm^{-2} and a FWHM of 596 km s^{-1} after correction for the finite spectral resolution. (9) $Pa\beta$ is contaminated by He I λ1.27887 with a flux of 1.79×10^{-14} ergs s^{-1} cm^{-2} and a FWHM of 582 km s^{-1} after correction for the finite spectral resolution.

[a] Durret & Bergeron 1988.
[b] Véron et al. 1980.
[c] Dahari & De Robertis 1988.
[d] Veilleux 1991a.
[e] Whittle 1992.
[f] Goodrich 1992.
[g] Armus, Heckman, & Miley 1989.
[h] Vrtilek & Carleton 1985.
[i] De Robertis & Osterbrock 1986.
[j] Osterbrock 1985.
[k] Cruz-Gonzalès et al. 1994.
[l] Whittle 1985.
[m] Bergvall et al. 1986.
[n] Shields & Filippenko 1990.
[o] Terlevich et al. 1991.
[p] Moorwood & Oliva 1988.
[q] Sharples et al. 1984.

exception to this rule of thumb is NGC 2110, where a conservatively high upper limit of one-half the narrow Hα flux was used. Finally, lower limits to A_V in objects with only upper limits to broad Paβ, Brγ, or Brα were derived using the method described in Paper I (giving $A_V > 11$ for Paβ, > 26 for Brγ, and > 68 for Brα). The intrinsic ratios assumed for the calculations are listed in Table 2. These values of the extinction may be compared with those derived from X-ray measurements, A_V(X-ray) (see Table 5). Since A_V(IR) measures the extinction due to dust while A_V(X-ray) measures the strength of absorption edges associated with oxygen or iron ions, these values will not necessarily agree. The A_V(IR)/A_V(X-ray) ratio will depend not only on the dust-to-gas ratio and the metallicity of the gas but also on the detailed distribution of the ionized component with respect to the neutral component. For example, in the highly stratified wind model of Königl & Kartje (1994), the warm dust-free inner region of the wind is likely to dominate the X-ray opacity at all but very large θ ($\lesssim 80°$; see their Fig. 6). This model can therefore naturally explain the existence of objects in which the nuclear X-rays are strongly absorbed but the BLR is directly observable (see, e.g., Nandra & Pounds 1992; Nandra et al. 1993; Turner et al. 1993a, 1993b; Fiore et al. 1993). Note also that gas between the BLR and the nuclear source is not accounted for in A_V(IR) but is in A_V(X-ray).

Figure 3 displays the values of A_V(IR) as a function of A_V(X-ray) for our sample galaxies. We confirm the slight tendency for the objects with broad Paβ and Brγ to have the lowest X-ray column depths (see Paper I). This statement is based on only a few objects, and it therefore needs to be confirmed when infrared spectra with high S/N become available for a larger number of Seyfert 2 galaxies. Considering the large uncertainties in the X-ray and infrared measurements, the X-ray extinctions do not show any significant trend to be systematically larger than the infrared BLR extinctions. In fact, the opposite seems to be true in NGC 1068, NGC 2992, NGC 5506, and MCG −05-23-16. In NGC 1068, the observed X-rays are almost certainly not seen through the torus but instead represent a scattered component; the same phenomenon may be taking place in NGC 2992, NGC 5506, and MCG −05-23-16, and even perhaps in other galaxies (Mulchaey, Mushotzky, & Weaver 1992). If that is the case, A_V(X-ray) is not a good measure of the extinction towards the nucleus, and only A_V(IR) should be considered for this purpose.

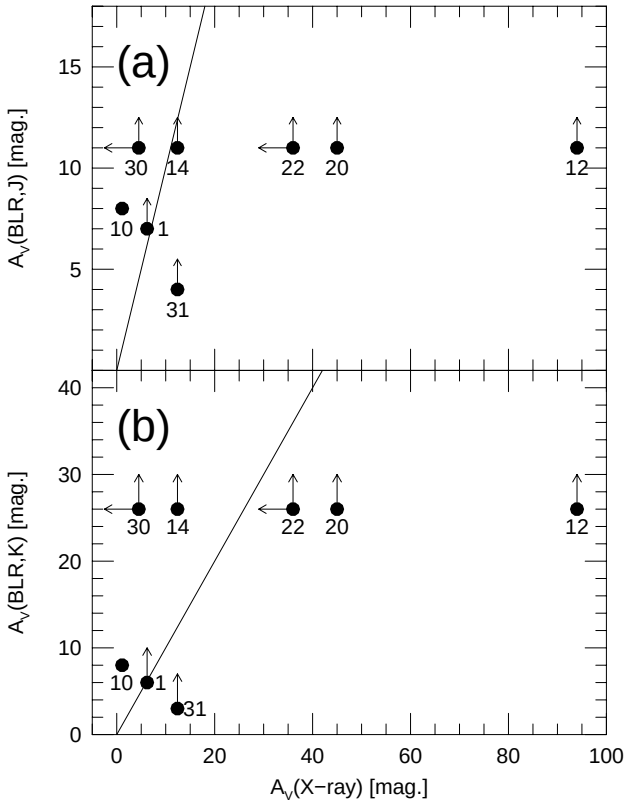

FIG. 3.—Broad-line extinctions determined from the infrared spectra as a function of the extinctions derived from the X-ray column depths. The broad-line extinctions were determined from (*a*) Paβ$_b$/Hα$_b$; (*b*) Brγ$_b$/Hα$_b$. The numbers identify individual objects following the order in Table 1. The solid lines represent the equality lines. Mrk 3 lies at position (319, $\gtrsim$11) in the top figure.

Mid-infrared data also exist for six objects in our sample. We list in column (7) of Table 5 the visual extinctions to the 10 μm source derived from the strength of the 9.7 μm silicate feature, A_V(9.7). The value of the A_V(9.7)/τ(9.7) ratio is known to vary in our Galaxy according to the metallicity of the medium (Roche & Aitken 1985). The ratio used in Table 5 is intermediate between that in solar neighborhood and that along the line of sight to the galactic center (Roche et al. 1986). The value of A_V(9.7) is either similar to or lower than A_V(IR). It is important to use caution when interpreting the values of A_V(9.7) since the use of the 9.7 μm silicate feature as a measure of the extinction in Seyfert galaxies has been put into question by a number of researchers. For instance, Pier & Krolik (1992b, 1993) argue that the strength of 9.7 μm feature depends on orientation, with a possible tendency for absorption features to be more prominent in edge-on tori than in face-on tori. The silicate feature is sometimes seen in emission in some Seyfert galaxies and is clearly not a good measure of the extinction in those cases. The extinctions based on the silicate feature should therefore be considered only illustrative.

The possibly important fraction of Seyfert 2's in our sample with detected broad near-infrared lines (perhaps as large as ∼25%) suggests that partially obscured Seyfert 2 galaxies are not uncommon. These objects are easy to explain in the context of the molecular torus model of Pier & Krolik (1992a) if one postulates that the "skin" of the torus—the transition zone between the optically thin "throat" of the torus and the optically thick core—is extended and devoid of dust. This slight modification to the standard torus model would also explain the existence of "intermediate" Seyferts (1.8's and 1.9's) in which faint optically detected BLRs present large reddenings ($2 \lesssim A_V \lesssim 5$; see Goodrich 1995 and references therein for a complete discussion). Careful calculations of the space densities of these intermediate Seyferts relative to Seyfert 1's and 2's imply that the region of intermediate optical depth extends over the range of polar angles $35° \lesssim \theta \lesssim 55°$ (Osterbrock & Shaw 1988; Osterbrock & Martel 1993; Maiolino & Rieke 1995). As pointed out by Königl & Kartje (1994), these results can easily be explained in the dusty wind model (see their Fig. 5).

In contrast, the thin warped disk model of quasars seems to run into a number of problems when applied to Seyfert galaxies. The large X-ray column densities and/or the lack of broad lines at Brα in some of our sample galaxies (e.g., Mrk 3 and NGC 4388) suggest the existence of highly opti-

cally thick material ($A_V > 50$) in at least some Seyfert 2 galaxies. The large X-ray columns detected in NGC 4507 and IRAS 18325−5962 would also place them in this category (see, e.g., Awaki et al. 1991). Such large column depths are difficult to explain with a thin warped disk. The existence of a kiloparsec-scale, nonaxisymmetric disk in Seyfert galaxies also seems inconsistent with the observed morphology and size of the projected ionization cones.

The present data can be used to put constraints on the location of the dust producing the reddening observed in the BLR. To address this issue, the broad-line extinctions, or their lower limits, are compared with the narrow-line extinctions listed in Tables 3 and 4. The narrow-line extinctions are at least 1 mag smaller than the broad-line extinctions, even when using conservatively high values of the narrow-line extinctions (see Table 5 and Fig. 4). The larger extinction to the BLR places the majority of the dust between the NLR and BLR, or mixed in with the BLR (although this second possibility is considered less likely based on theoretical arguments; see, e.g., Laor & Draine 1993; Netzer & Laor 1993). A similar conclusion was reached by Goodrich (1995), based on intermediate Seyfert variability timescales, and by Hill et al. (1996), using infrared spectra of radio galaxies. These results are consistent with the torus and dusty wind models but are more difficult to explain with a thin warped disk.

4.2. [Fe II] *Emission*

The ionization potentials of neutral and singly ionized Fe are 7.87 and 16.16 eV, respectively. [Fe II] emission is therefore produced predominantly in regions in which hydrogen is only partially ionized. These zones are virtually absent in ordinary H II regions, where the transition between fully ionized and neutral hydrogen gas is very sharp. Yet, many starburst galaxies present strong [Fe II] emission (see, e.g., Mouri et al. 1990, 1993; Moorwood & Oliva 1988, 1990; Kawara et al. 1988; Colina 1993; Puxley et al. 1994). There is a growing consensus that the [Fe II] emission in these objects is produced in the cooling tails of supernova remnants (SNRs). Detailed studies of a few nearby starbursts indicate a direct spatial coincidence between the sites of [Fe II] and 6 cm radio emission (see, e.g., Lester et al. 1990; Clegg et al. 1991; Greenhouse et al. 1991; Forbes et al. 1993; van der Werf et al. 1993; Forbes & Ward 1994). Photodissociation regions are probably responsible for only a small fraction of the total [Fe II] emission in these objects (Mouri et al. 1993; see Burton, Hollenbach, & Tielens 1990, however).

The origin of the strong [Fe II] emission in AGNs is more ambiguous. A number of processes may contribute to the emission in these galaxies: (1) X-rays from the central source may produce extensive partially ionized regions in NLR clouds of high optical depths; (2) starburst activity may be taking place in or near the nucleus of these galaxies; (3) the interaction of radio jets with the surrounding medium may induce shocks and produce partially ionized cooling tails. An excellent way to differentiate between these various processes is to compare the spatial distributions of [Fe II] and radio emission. One of the few Seyfert galaxies imaged to date at these wavelengths is NGC 1068 (Blietz et al. 1994). In this object, the morphology of the [Fe II] emission correlates with that of the radio jet, supporting scenario (3). Evidence for jetlike radio emission exists in most of our sample galaxies. However, without spatial information on the [Fe II] emission, it is difficult to say whether jet-induced shocks are sufficiently widespread in our galaxies to explain the strong [Fe II] emission.

Until [Fe II] maps become available for our sample galaxies, we therefore have to rely on the strength and profile of the integrated nuclear [Fe II] line emission to determine the origin of [Fe II]. In the pure starburst scenario, the

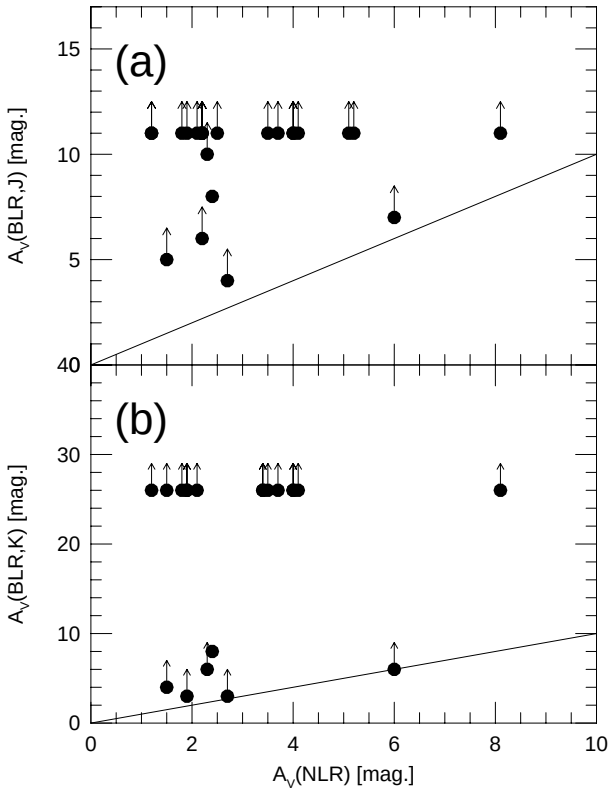

FIG. 4.—Broad-line extinctions as a function of the maximum narrow-line extinctions. The broad-line extinctions were determined from (*a*) $Pa\beta_b/H\alpha_b$; (*b*) $Br\gamma_b/H\alpha_b$. The numbers identify individual objects following the order in Table 1. The solid lines represent the equality lines.

TABLE 4

L-BAND LINE MEASUREMENTS

			$E(B-V)_n$			
OBJECT (1)	$Br\alpha_n$ (2)	$Br\alpha_b$ (3)	$H\alpha/H\beta$ (4)	$Pa\beta/H\alpha$ (5)	$Br\gamma/H\alpha$ (6)	$Br\alpha/H\alpha$ (7)
NGC 4388.....	8.54	...	0.58	1.10	0.75	1.14
	416	...				
	298	...				
NGC 5506.....	31.6	...	0.82	2.61	1.91	1.71
	605	...				
	531	...				

NOTE.—For each emission line of each object, we list the observed line flux in 10^{-14} ergs s^{-1} cm^{-2} on the first row, the observed line width in km s^{-1} on the second row, and the line width corrected for the instrumental resolution in km s^{-1} on the third row. Col. (1): Name of object. Cols. (2)–(3): Line fluxes and line widths for narrow Brα and broad Brα, respectively. Cols. (4)–(7):Narrow-line color excesses derived using

$$E(B-V)\left(\frac{\text{line 2}}{\text{line 1}}\right) = \frac{2.5}{[A_1/E(B-V)]+[A_2/E(B-V)]} \log\left[\frac{(F_2/F_1)}{(F_2/F_1)_0}\right]$$

with the intrinsic flux ratios and interstellar extinction coefficients listed in Table 2.

TABLE 5

X-RAY AND INFRARED OPTICAL DEPTH ESTIMATES IN SEYFERT 2 GALAXIES

Object (1)	log N_H (2)	A_V(X-ray) (3)	$A_V(J0)$ (4)	$A_V(K)$ (5)	$A_V(L)$ (6)	$A_V(9.7)$ (7)	$A_V(\mathrm{NLR})_{max}$ (8)	References (9)
MCG −05-23-16	$22.14^{+0.08}_{-0.08}$	6.2	$\gtrsim 7$	$\gtrsim 6$	...	6	6.0	2, 4
Mrk 3	$23.85^{+0.10}_{-0.10}$	319	$\gtrsim 11$	...	...	...	2.2	1
Mrk 78	...	...	$\gtrsim 11$	...	...	...	2.2	...
Mrk 176	...	...	$\gtrsim 6$	::[a]	...	...	2.2	...
Mrk 266SW	...	...	$\gtrsim 11$	$\gtrsim 26$	...	...	4.1	...
Mrk 266NE	...	...	$\gtrsim 11$	...	...	...	5.1	...
Mrk 463E	...	...	$\gtrsim 10$	$\gtrsim 6$	...	...	2.3	...
Mrk 477	...	...	$\gtrsim 11$	$\gtrsim 3$	...	...	1.9	...
Mrk 1388	...	...	$\gtrsim 11$	...	...	...	2.2	...
NGC 2992	$21.37^{+0.23}_{-0.30}$	1.1	~ 8	~ 8	...	3	2.4	2, 4
NGC 3081	...	...	::	...	...	...	4.4	...
NGC 4388	$23.32^{+0.37}_{-0.47}$	94	$\gtrsim 11$	$\gtrsim 26$	$\gtrsim 68$	...	3.5	3
NGC 5252	...	...	...	...	...	...	...	...
NGC 5506	$22.44^{+0.08}_{-0.07}$	12.4	$\gtrsim 11$	$\gtrsim 26$	$\gtrsim 68$	20	8.1	2, 5
NGC 5728	...	...	::	...	...	...	1.9	...
Akn 79	...	...	...	::	...	...	2.9	...
ESO 428-614	...	...	$\gtrsim 11$	...	...	...	1.2	...
IC 5135	...	...	...	$\gtrsim 26$	...	...	3.4	...
Mrk 1	...	...	...	$\gtrsim 26$	...	...	1.9	...
Mrk 348	$23.00^{+0.10}_{-0.10}$	45	$\gtrsim 11$	$\gtrsim 26$	...	0	2.1	1, 5
Mrk 403	...	...	$\gtrsim 11$	...	...	...	2.5	...
Mrk 533	<22.9	<36	$\gtrsim 11$	$\gtrsim 26$	...	4	4.0	1, 4
Mrk 573	...	...	$\gtrsim 11$	$\gtrsim 26$	...	...	1.8	...
Mrk 622	...	...	$\gtrsim 11$	...	...	...	5.2	...
Mrk 917	...	...	...	$\gtrsim 26$	...	...	3.4	...
Mrk 1066	...	...	$\gtrsim 11$	$\gtrsim 26$	...	...	3.7	...
Mrk 1073	...	...	$\gtrsim 11$	$\gtrsim 26$	...	...	4.0	...
Mrk 1157	...	...	...	$\gtrsim 26$	...	...	1.9	...
Mrk 1210	...	...	$\gtrsim 5$	$\gtrsim 4$	...	...	1.5	...
NGC 1068	<22.0	<4.5	$\gtrsim 11$	$\gtrsim 26$	$\gtrsim 68$[b]	8	1.2	1, 5
NGC 2110	$22.44^{+0.31}_{-0.55}$	12.4	$\gtrsim 4$	$\gtrsim 3$	...	≤ 11	2.7	2, 5
NGC 7172	...	...	...	::	...	...	$\gtrsim 2.5$	...
NGC 7212	...	...	...	$\gtrsim 26$	...	...	1.5	...

NOTE.—Col. (1): Object name. Col. (2): Effective neutral column density derived from either *Ginga*, *SL2 XRT* (NGC 4388), or *HEAO* data, with the former source being preferred when available. Col. (3): Extinction derived using the empirical relationship of Gorenstein 1975 between the visual extinction and column densities in sources in our own Galaxy. Col. (4): Extinction determined from the ratio of the broad components in Paβ and Hα assuming Case B recombination and $A_V = 3.1\ E(B-V)$. Col. (5): Extinction determined from the ratio of the broad components in Brγ and Hα assuming Case B recombination and $A_V = 3.1\ E(B-V)$. Col. (6): Extinction determined from the ratio of the broad components in Brα and Hα assuming Case B recombination and $A_V = 3.1\ E(B-V)$. Col. (7): Extinction determined from the depth of the 9.7 μm silicate feature using $A_V(9.7\mu\mathrm{m}) = 15\ \tau_{9.7}$ and a simple power-law fit to the continuum. Col. (8): Conservatively high value of the extinction toward the narrow-line region determined from the color excesses listed in Tables 3 and 4 and assuming $A_V = 3.1\ E(B-V)$. Col. (9): References to the X-ray and 9.7μm data.—(1) Turner et al. 1991; (2) Aitken & Roche 1985; (3) Awaki et al. 1991; (4) Hanson et al. 1990; (5) Roche et al. 1984.

[a] Double colons mean that the intensity of the broad component of this hydrogen recombination line is too uncertain to derive an extinction.

[b] From the absence of broad Brα in the spectra of DePoy 1987.

emission from [Fe II] is produced through shocks in supernova remnants and is therefore regulated by the supernova rate, while the hydrogen recombination lines are produced by photoionization and relate mostly to the content of massive, young, and unevolved main-sequence hot stars (see, e.g., Moorwood & Oliva 1988). The ratio of [Fe II] emission relative to hydrogen recombination line emission is thus very sensitive to changes in the IMF slope and on the upper mass limit. Detailed calculations by Colina (1993) have shown, however, that the starburst scenario has difficulties explaining [Fe II] λ1.64/Brγ larger than $\sim$1.4 or, equivalently, [Fe II] λ1.257/Paβ larger than $\sim$0.4. Most of our sample galaxies have [Fe II]/Paβ ratios that lie above this limit. This result suggests that circumnuclear starbursts are not the main source of [Fe II] emission in our Seyfert galaxies.

In Paper I, we tentatively confirmed the existence of a correlation between [Fe II]/Paβ and [O I] λ6300/Hα in AGN and starburst galaxies (Mouri et al. 1990). The complete data set on our Seyfert 2 galaxies is plotted in Figure 5 along with the data of Mouri et al. The references to the optical line ratios in the Seyfert 2 galaxies are listed in Table 6. Only the narrow components of Paβ and Hα were used for this analysis. Once again, a correlation between [Fe II]/Paβ and [O I] λ6300/Hα is detected, but this correlation is only marginal within the class of AGNs. Among the Seyfert 2 galaxies of our sample, the probability, P[null], that this correlation is fortuitous is roughly 1%. As discussed in Paper I, the correlation in Figure 5 trivially implies that both [O I] and [Fe II] emission come from partially ionized regions but does not help us discriminate between the various processes responsible for the existence of these regions. The lack of correlation between the line widths of [Fe II] λ1.2567 and Paβ noted in § 3 (or between the line widths of [Fe II] and Hα; Fig. 6) is further evidence that the [Fe II] line–emitting region does not coincide with the fully ionized narrow-line region producing the hydrogen recombination lines.

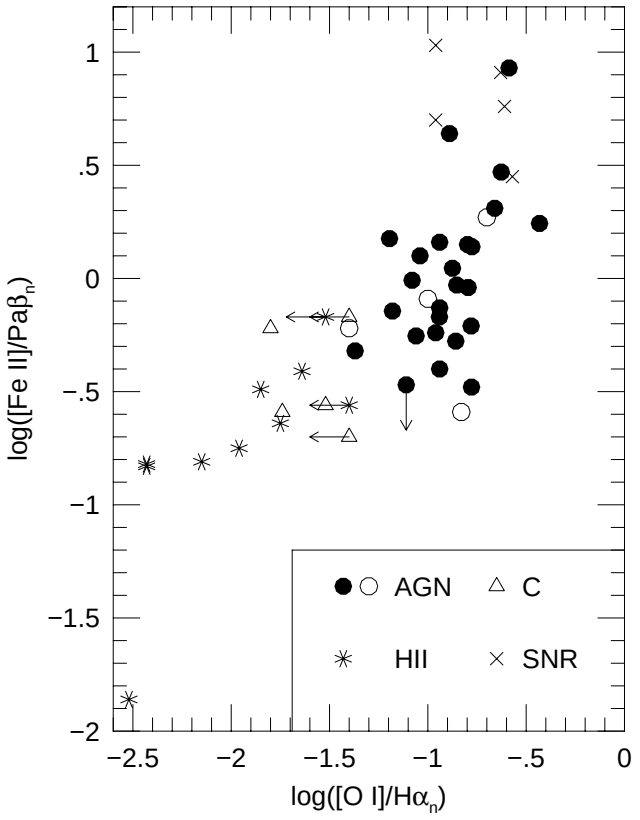

FIG. 5.—[Fe II] λ1.2567/Paβ_n flux ratios as a function of [O I] λ6300/Hα_n flux ratios. The filled circles are the data from the present paper. The other symbols are from the compilation of Mouri et al. (1990). Circles are AGNs, crosses are supernova remnants, triangles are composite systems that show evidence for both AGNs and starburst activity, and stars are starburst galaxies, except for the data point at the lower left, which is the Orion Nebula. A correlation is observed among the whole sample but is barely significant when only AGNs are considered.

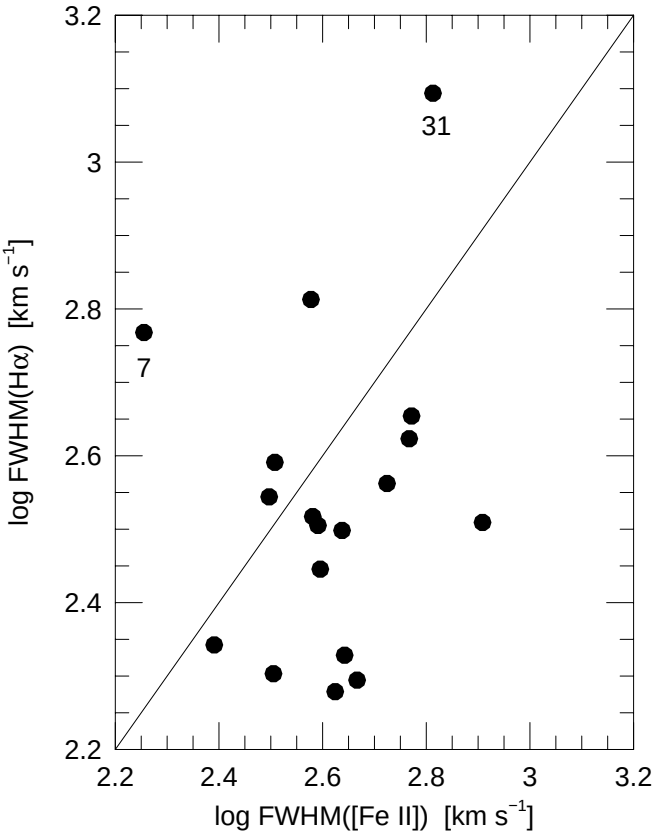

FIG. 6.—Line widths of narrow Hα as a function of line widths of [Fe II] λ1.2567. The solid line represents the equality line. The numbers identify individual objects following the order in Table 1. No correlation is present, which suggests that these lines originate in a different volume of gas.

In the photoionization scenario, one might expect a correlation between the [Fe II] emission and the X-ray flux emitted from the active nuclei. Using the X-ray fluxes listed in Table 6, neither the soft (0.2–4 keV) nor the hard (2–10 keV) X-ray components of our sample galaxies correlate significantly with the strength of [Fe II] (Fig. 7; P[null] $\gtrsim$ 4%). However, this lack of correlation does not allow us to discard scenario (1) since, strictly speaking, the [Fe II] emission produced through photoionization is expected to correlate only with the soft X-ray flux *incident* on the NLR clouds, not with the X-ray component that reaches the telescope. The absence of a correlation might simply reflect variations in the effective covering factor from one galaxy to the next. Indeed, the fact that the [Fe II] emission increases with increasing far-infrared emission (Fig. 8) may indicate that the strength of the [Fe II] feature is related to the fraction of the radiation emerging from the nucleus that is absorbed and reprocessed by nearby optically thick clouds.

As first pointed out by Forbes & Ward (1993), perhaps a more serious hurdle for the photoionization hypothesis is the fact that the [Fe II] emission in both starbursts and AGNs follow a similar relation with radio emission. This correlation is present for both the 20 cm and 6 cm radio fluxes (Fig. 9; P[null] = 0.004% and 0.009%, respectively) and implies a close relationship between the source of the synchrotron emission and the source of the [Fe II] emission. Fast shocks induced by the interaction of material out-

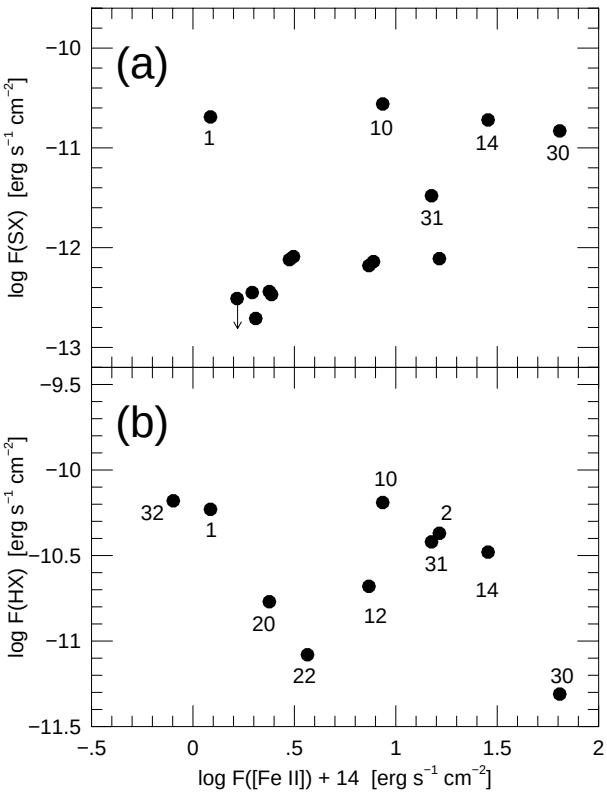

FIG. 7.—X-ray fluxes as a function of [Fe II] λ1.2567 fluxes. (*a*) 0.2–4 keV; (*b*) 2–10 keV. The numbers identify individual objects following the order in Table 1.

TABLE 6

PROPERTIES OF SAMPLE GALAXIES

Object (1)	Redshift (2)	$F_{6\ cm}$ (3)	$F_{20\ cm}$ (4)	F_{FIR} (5)	log (SX) (6)	log (HX) (7)	log (O I/Hα) (8)	log (Fe II/Paβ) (9)	log (H_2/Brγ) (10)	References (11)
MCG −05-23-16.....	0.0442	6.0	11.0	...	−10.69	−10.23	−0.78	−0.21	...	1/2/1/.../3/3/4
Mrk 3	0.0139	353	1100	68.10	−12.11	−10.37	−0.798	0.15	...	5/6/1/7/3/3/8
Mrk 78	0.0375	12	31	15.48	−12.45	...	−0.94	0.16	...	1/9/9/7/3/3/10,11
Mrk 176	0.0269	10.4	21.0	12.33	< −12.51	...	−0.89	0.64	...	1/9/1/7/3/.../10
Mrk 266SW	0.0276	10.1	32.4	68.37	...	...	−1.37	−0.32	−0.121	1/12/12/7/.../.../13,14
Mrk 266NE	0.0276	12.2	23.5	68.37	...	...	−1.04	0.10	...	1/12/12/7/.../.../13,14
Mrk 463E	0.0501	100	322.5	40.81	−12.71	...	−0.941	−0.17	−0.282	1/15/15/7/3/../16
Mrk 477	0.0373	25.0	58.	17.24	−12.14	...	−0.94	−0.13	0.019	1/9/1/7/3/.../11,16
Mrk 1388	0.0213	3.5	9.11	<7.76	...	...	−0.94	−0.40	...	1/17/17/7/.../.../18
NGC 2992	0.0079	77.0	206	107.4	−10.56	−10.19	−0.627	0.47	0.604:	1/2/2/7/3/3/4
NGC 3081	0.0081	0.9	2.5	...	−12.09	...	−0.96	−0.24	...	1/19/19/.../3/.../20
NGC 4388	0.0081	93	150	136.5	−12.18	−10.68	−0.795	−0.04	0.216	5/6/1/7/3/3/21
NGC 5252	0.0234	11.6	15.2	...	...	...	...	0.26	...	22/23/23/.../.../.../...
NGC 5506	0.0063	160	320	120.2	−10.72	−10.48	−0.778	−0.48	...	5/2/2/7/3/3/8
NGC 5728	0.0101	4.6	100	78.14	−12.12	...	−0.776	0.14	0.499	1/19/1/7/3/.../21
Akn 79	0.014	...	12.	...	...	...	−0.699	...	> −0.27::	1/.../1/.../.../.../16
ESO 428-614	0.0048	28.2	70.1	<24.58	...	...	−0.875	0.045	...	24/19/19/7/.../.../24
IC 5135.....	0.0160	...	...	155.8	...	...	−1.049	...	0.098	25/.../21/7/.../.../26
Mrk 1	0.0161	32	68.	<71.08	< −12.32	...	−0.623	...	0.0442	1/6/1/7/3/.../10
Mrk 348	0.0151	254	340	24.11	−12.44	−10.77	−0.432	0.243	0.125	1/6/1/7/3/3/10
Mrk 403	0.0244	...	...	...	...	...	−1.11	< −0.470	...	1/.../.../.../.../.../.../27
Mrk 533	0.0292	...	220	74.57	...	−11.08	−1.06	−0.254	−0.491	5/.../1/7/.../.../27
Mrk 573	0.0171	5.5	11.	<22.17	−12.47	...	−0.853	−0.029	−0.311	1/9/1/7/3/.../28
Mrk 622	0.0228	...	9.30	<16.85	...	...	−1.195	0.176	...	1/.../1/7/.../.../16
Mrk 917	0.0242	...	...	37.98	...	...	−1.02	...	0.076	1/.../.../7/.../.../28
Mrk 1066	0.0123	35.5	94.3	104.4	...	...	−1.08	−0.008	0.0032	5/19/19/7/.../.../27
Mrk 1073	0.0236	44	150	81.52	...	...	−1.18	−0.144	−0.0781	5/6/29/7/.../.../27
Mrk 1157	0.0150	7.9	24.5	23.39	...	...	−0.865	...	0.260	5/19/19/7/.../.../10
Mrk 1210	0.0135	56	...	42.76	...	...	−0.660	0.31	−0.24	30/6/.../7/.../.../31
NGC 1068	0.0036	1090	3800	2983.	−10.83	−11.31	−0.858	−0.09[a]	0.06[b]	1/2/2/7/3/3/8
NGC 2110	0.0076	175	270	45.56	−11.48	−10.42	−0.587	0.91	0.594	5/2/2/7/3/3/8
NGC 7172	0.0085	1.8	20	66.12	...	−10.18	...	...	> −0.248	32/24/34/7/.../3/...
NGC 7212	0.0264	46	...	34.05	...	...	−0.774	...	−0.141	1/6/.../7/.../.../28

NOTE.—Col. (1): Object name. Col. (2): Redshift. Col. (3): Flux at 6 cm in mJy. Col. (4): Flux at 20 cm in mJy. Col. (5): Far-infrared flux in 10^{-11} ergs s^{-1} cm^{-2} determined using the method of Kim et al. 1995. Col. (6): Logarithm of total observed *Einstein* flux between 0.2 and 4 keV in ergs s^{-1} cm^{-2}. Col. (7): Logarithm of total 2–10 keV flux corrected for observed absorption in ergs s^{-1} cm^{-2}. Col. (8): Logarithm of the narrow-line flux ratio F([O I] λ6300)/F(Hα_n). Col. (9): Logarithm of the narrow-line flux ratio F([Fe II] λ1.257)/F(Paβ_n). Col. (10): Logarithm of the narrow-line flux ratio $F(H_2\ \lambda 2.122)/F(Br\gamma_n)$. Col. (11): References to data in Cols. (2)–(8).

[a] Kawara, Nishida, & Taniguchi 1988.

[b] Moorwood & Oliva 1990.

REFERENCES—(1) Dahari & De Robertis 1988; (2) Ulvestad & Wilson 1984b; (3) Mulchaey et al. 1994; (4) Durret & Bergeron 1988; (5) Veilleux 1991b; (6) Gregory & Condon 1991; (7) Fluxes of Moshir et al. 1992 and prescription described in Kim et al. 1995; (8) Veilleux 1991c; (9) Ulvestad & Wilson 1984a; (10) Koski 1978; (11) De Robertis 1987; (12) Mazzarella et al. 1988; (13) Armus et al. 1989; (14) Kollatschny & Fricke 1984; (15) Mazzarella et al. 1991; (16) Shuder & Osterbrock 1981; (17) Ulvestad et al. 1995; (18) Osterbrock 1985; (19) Ulvestad & Wilson 1989; (20) Durret & Bergeron 1986; (21) Phillips, Charles, & Baldwin 1983; (22) Tadhunter & Tsvetanov 1989; (23) Wilson & Tsvetanov 1994; (24) Bergvall et al. 1986; (25) Sandage & Tammann 1987; (26) Shields & Filippenko 1990; (27) Veilleux & Osterbrock 1987; (28) Durret 1994; (29) Whittle 1992; (30) Hewitt & Burbidge 1991; (31) Terlevich et al. 1991; (32) Sharples et al. 1984; (34) Unger et al. 1987.

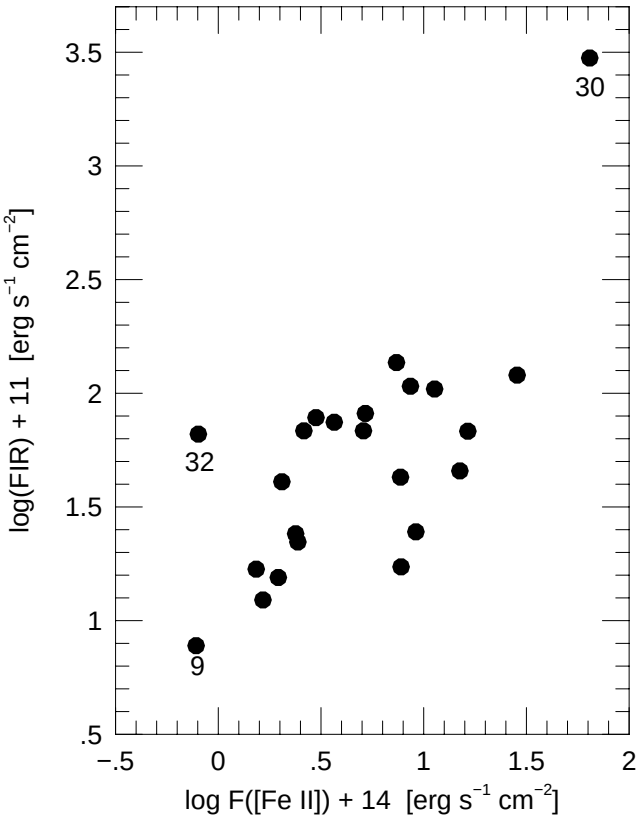

FIG. 8.—Far-infrared fluxes as a function of [Fe II] λ1.2567 fluxes. The numbers identify individual objects following the order in Table 1.

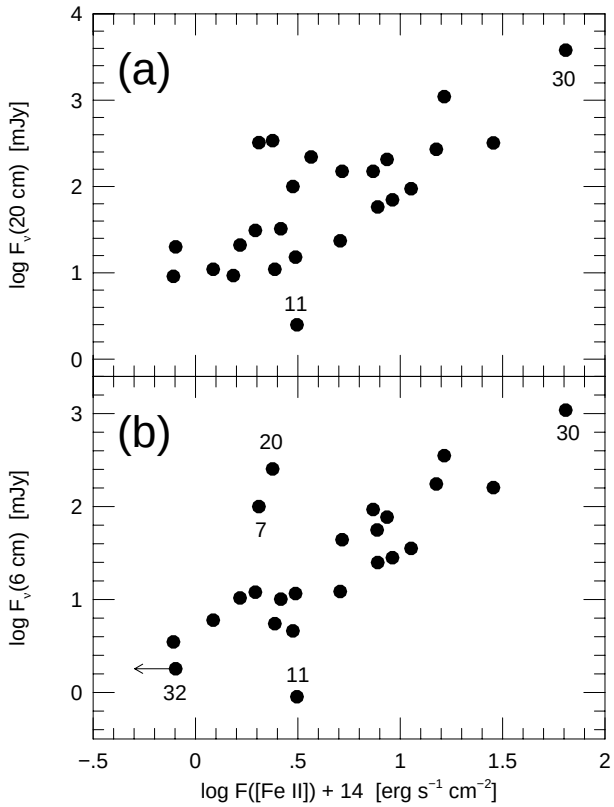

FIG. 9.—Radio fluxes as a function of [Fe II] λ1.2567 fluxes. (*a*) 20 cm; (*b*) 6 cm. The numbers identify individual objects following the order in Table 1. A correlation is observed in both figures.

flowing from the nucleus and colliding with the ambient gas (scenario [3]) can explain this correlation. In contrast, no *direct* relationship between the radio emission and the low-ionization line emission is expected in scenario (1). Studies at optical wavelength may provide a solution to this problem, however. For many years now, a correlation between the optical [O III] λ5007 emission and the radio power has been known to exist (see, e.g., Wilson & Willis 1980). These data are often explained with hybrid models in which the radio emission is produced through shocks and the line emission is produced in postshock gas that is kept ionized by the nuclear UV continuum (Whittle et al. 1988; Taylor, Dyson, & Axon 1992; Veilleux 1991c; see, however, Dopita & Sutherland 1995). It is possible that similar processes can explain the correlation between [Fe II] and radio emission.

Difficulties with pure shock models also exist. First, it is not clear whether the [Fe II]/Paβ ratio produced through shocks is sufficiently large to simulate the ratios in our Seyfert 2 galaxies. As discussed earlier, typical shocks in SNRs seem to underproduce [Fe II] relative to Paβ. We are not aware of any published attempts to determine the [Fe II]/Paβ ratio from shocks induced by nuclear outflows. If outflow-induced shocks are to explain the [Fe II] emission in Seyfert 2 galaxies, one must also demonstrate that the efficiency in producing [Fe II] emission through this process relative to the radio emission is similar to that in SNRs (Forbes & Ward 1993). Finally, pure shock models predict a correlation between line widths and emission-line luminosities (see, e.g., Dopita & Sutherland 1995). Figure 10 does not show any clear tendency for the luminosity in the

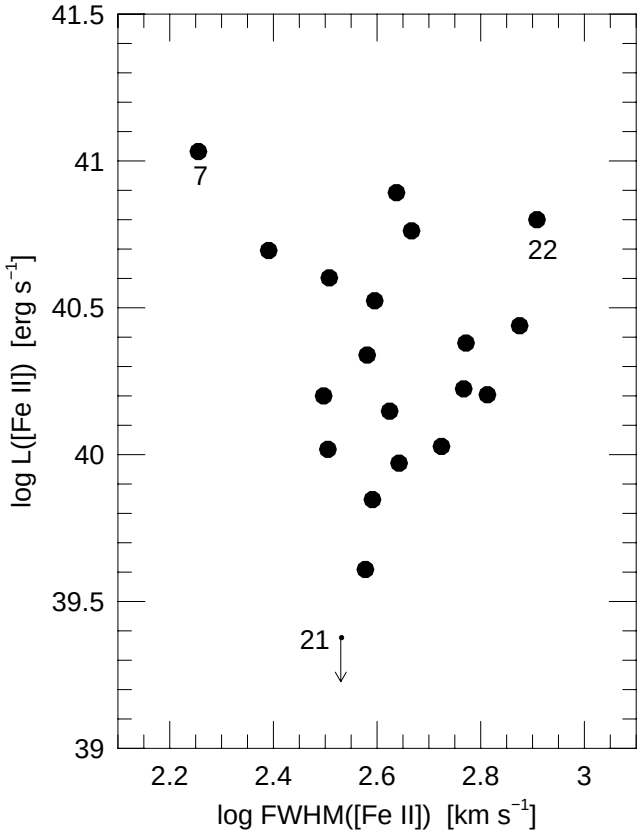

FIG. 10.—[Fe II] λ1.2567 luminosities as a function of [Fe II] line widths. The numbers identify individual objects following the order in Table 1. No significant trend is observed.

[Fe II] line to increase with the [Fe II] line widths. Although this result needs to be confirmed with data of higher resolution, this lack of correlation is difficult to explain with shock models unless the environment (e.g., preshock gas density) varies significantly from one galaxy to the other. Measurements of the electron temperature in the [Fe II] line–emitting region would also help clarify the role of shocks (Mouri et al. 1993; Thompson 1995). Unfortunately, as discussed in detail in Paper I, none of the weaker [Fe II] lines that lie in the *J*-band are both sensitive enough to temperature variations and strong enough to be measured in the spectra of our Seyfert 2 galaxies.

In summary, the present data rule out a purely starburst origin for the [Fe II] emission in Seyfert galaxies. Shocks associated with nuclear outflows are a likely source of [Fe II] emission, although photoionization by the nuclear continuum may also contribute to the emission.

4.3. *Emission from Molecular Hydrogen*

Emission from molecular hydrogen is observed in most of the galaxies in our sample for which we have *K*-band data. The H_2 masses that we derive from the H_2 λ2.121 luminosities range from 100 to 10,000 $M_\odot$ (see § 3). There are two basic ways to excite molecular hydrogen: collisional excitation, i.e., inelastic collisions between molecules in a warm gas ($\gtrsim$1000 K), or fluorescent excitation through absorption of soft-UV radiation (912–1108 Å) in the Lyman and Werner bands. The method most commonly used to differentiate collisional excitation from fluorescence consists in using flux ratios of various H_2 lines visible in the *K* band, particularly the H_2 $v = 1$–0 $S(1)$ 2.12125 μm, $v = 1$–0 $S(0)$ 2.2227 μm, and $v = 2$–1 $S(1)$ 2.2471 μm transitions. In the case of purely radiative UV fluorescence excitation (i.e., UV excitation at low densities), H_2 2–1 $S(1)$/1–0 $S(1)$ is expected to be 0.5–0.6 and H_2 1–0 $S(0)$/1–0 $S(1)$ is roughly 0.5 (see, e.g., Black & Dalgarno 1976; Black & van Dishoeck 1987; Sternberg 1988). In contrast, collisional excitation from a gas in thermal equilibrium at a temperature of 1000–4000 K produces H_2 2–1 $S(1)$/1–0 $S(1) \lesssim 0.35$ and H_2 1–0 $S(0)$/1–0 $S(1) \approx 0.2$–0.3 (Shull & Hollenbach 1978; Lepp & McCray 1983; Sternberg & Dalgarno 1989). Unfortunately, H_2 λ2.247 does not lie within the spectral coverage of our data, while H_2 λ2.223 is weak and often affected by absorption features from Na and Fe in the underlying stellar continuum. Nevertheless, constraints on the excitation process can still be derived from our data: the (admittedly few) objects with reliable H_2 1–0 $S(0)$ fluxes have H_2 1–0 $S(0)$/1–0 $S(1) \ll 0.5$. Although flux measurements of the H_2 2–1 $S(1)$ line are needed to draw any definite conclusions about the excitation process of H_2, our preliminary results appear to support previous studies which concluded that radiative fluorescence at low densities is not important in most AGNs and starburst galaxies (see, e.g., Fischer et al. 1987; Moorwood & Oliva 1990).

Three mechanisms may provide the heating necessary for collisional excitation of H_2 in our galaxies: (1) heating of dense photodissociation regions by UV radiation, (2) heating by X-rays from the AGNs, or (3) heating through shocks induced by nuclear outflows. A strong constraint on the importance of UV heating can be derived from the values of H_2 λ2.121/Brγ in our galaxies. Using only the flux from the narrow component of Brγ, H_2 λ2.121/Brγ typically is greater than unity. With the exception of the very uncertain measurement in NGC 1068, H_2 λ2.121 is never less than $\sim$50% the intensity of Brγ_n in any of our galaxies. This result seems to rule out UV heating from the central AGN since this process predicts H_2 λ2.121/Brγ considerably less than 0.5 for a broad range of spectral energy distributions and dust-to-gas ratios (Fischer et al. 1987; Moorwood & Oliva 1990; Kawara, Nishida, & Gregory 1990). Heating of dense photodissociation regions by UV radiation may be important in H II galaxies, however (Puxley, Hawarden, & Mountain 1990; Doyon, Wright, & Joseph 1994).

A comparison of the H_2 1–0 $S(1)$ and X-ray fluxes in our sample galaxies provides an excellent way to test the mechanism of X-ray heating. Indeed, the results of Lepp & McCray (1983) suggest that F_X(1–10 keV)/H_2 λ2.121 must be larger than 400 for X-ray heating to be a plausible excitation mechanism. Figure 11 shows the results of this comparison. With the exception of NGC 1068, all of the galaxies in our sample satisfy this criterion. (This criterion is likely to be satisfied even in NGC 1068 since the observed X-ray flux probably represents only a small fraction of the actual flux incident on the NLR clouds in this galaxy [see § 4.2].) A similar result was found by Kawara et al. (1990) in Seyfert 1's and quasars. Kawara et al. speculate that the H_2 emission in Seyfert 1's and quasars comes from the inner ($\leq$1 pc), spatially unresolved region of the molecular torus purported to exist in these objects (Krolik & Lepp 1989). Deep high-resolution H_2 maps are not available for most of our objects to test this scenario.

An important prediction of the X-ray heating hypothesis is that the intensity of the H_2 emission should correlate with

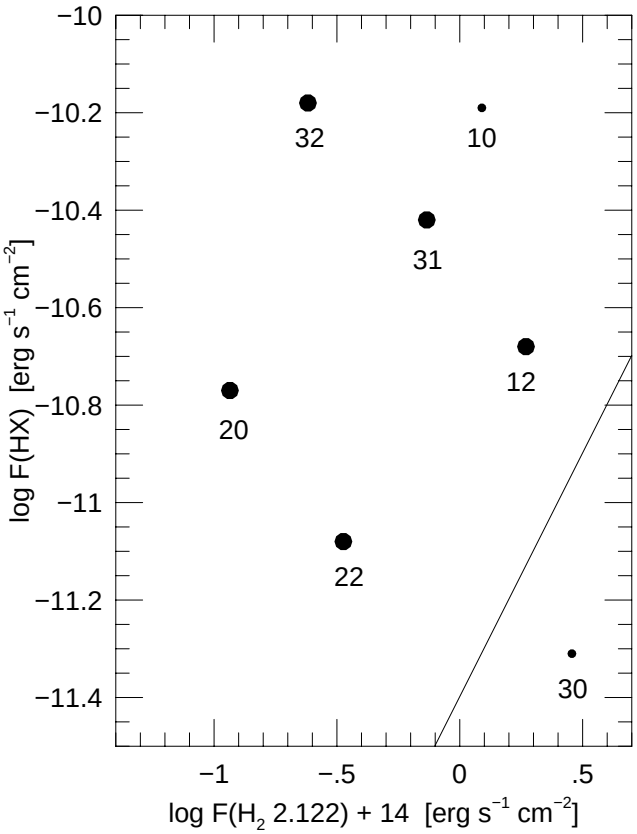

FIG. 11.—Hard (1–10 keV) X-ray fluxes as a function of H_2 λ2.121 fluxes. The numbers identify individual objects following the order in Table 1. The positions of the small symbols are uncertain. The solid line represents F(HX) = 400 F(H_2 2.121). All of the objects except NGC 1068 lie above this line.

the low-ionization emission produced in the partially ionized regions of optically thick NLR clouds. Figure 12 plots H_2 λ2.121/Brγ_n versus [O I] λ6300/Hα_n for our sample galaxies. The data points do not closely follow the relationship between H_2 and [O I] predicted by the photoionization model. This large scatter may indicate a wide range in the ratio of molecular to neutral atomic gas or the existence of an additional source of excitation in many of these objects. A similar result is found when H_2 λ2.121/Brγ_n is compared with [Fe II] λ1.2567/Paβ_n. Shock excitation by a nuclear-driven wind is often presumed to be responsible for the H_2 emission in NGC 1068 (see, e.g., Kawara et al. 1990; Oliva & Moorwood 1990; Moorwood & Oliva 1990; Blietz et al. 1994). There is now direct evidence that the same phenomenon may be taking place in NGC 7469 (Heckman et al. 1986), NGC 3079 (Hawarden et al. 1995), Centaurus A (Israel et al. 1990), and perhaps even in NGC 6240 (although *most* of the H_2 emission in this object is probably produced through shock excitation at the interface of the ISM of two merging galaxies: Herbst et al. 1990; van der Werf et al. 1993; Mouri & Taniguchi 1995). The scatter in Figure 12 may be attributable to shock excitation.

Kawara et al. (1987) found that the H_2 1–0 $S(1)$ emission normalized to the far-infrared emission is significantly enhanced in AGN as a group relative to starburst galaxies. They argue that the difference may be due to winds from the AGNs. Using the far-infrared fluxes listed in Table 6, we confirm the excess H_2 emission in the galaxies of our sample. With the exception of NGC 1068 in which aperture effects are very important, log (H_2 λ2.121/FIR) ranges from -4.3 (in Mrk 477) to -5.5, with the bulk of the objects having ratios in the narrow range (-4.7, -5.3). If shocks contribute significantly to the excitation of H_2 in these Seyfert 2 galaxies and if the bulk of the radio emission from these objects is also produced in (higher velocity) shocks associated with these nuclear outflows, one would expect a correlation between the strength of H_2 λ2.121 and radio emission. Figure 13 shows that the H_2 λ2.121 fluxes in our sample galaxies do indeed have a tendency to increase with 20 and 6 cm fluxes, but the correlations are less significant than for the [Fe II] emission (P[null] = 0.3% and 6.5% for Figures 13*a* and 13*b*, respectively; see previous section). A similar result was found by Forbes & Ward (1993).

The widths of the H_2 profiles are not correlated with and are generally smaller than the widths of [Fe II] λ1.2567 (Fig. 14). This difference in line widths may not be surprising, however, since dissociation of the H_2 molecules requires shock velocities only in excess of $\sim$25 km s^{-1} ($\sim$ 50 km s^{-1} if magnetic fields are present). In fact, the very detection of H_2 profiles with widths well above these velocities points to the importance of the effects associated with a multiphase ISM, where slow shocks are produced by high-velocity collisions between dense molecular cloudlets and a more ubiquitous, less dense gas phase (see, e.g., Heckman et al. 1986).

To first order, shock excitation of the H_2 molecules predicts a correlation between the shock velocities and the luminosities of H_2 λ2.121. Figure 15 shows that the widths of H_2 λ2.121 do *not* correlate with the H_2 luminosities, nor is there any clear correlation when the H_2 line widths are

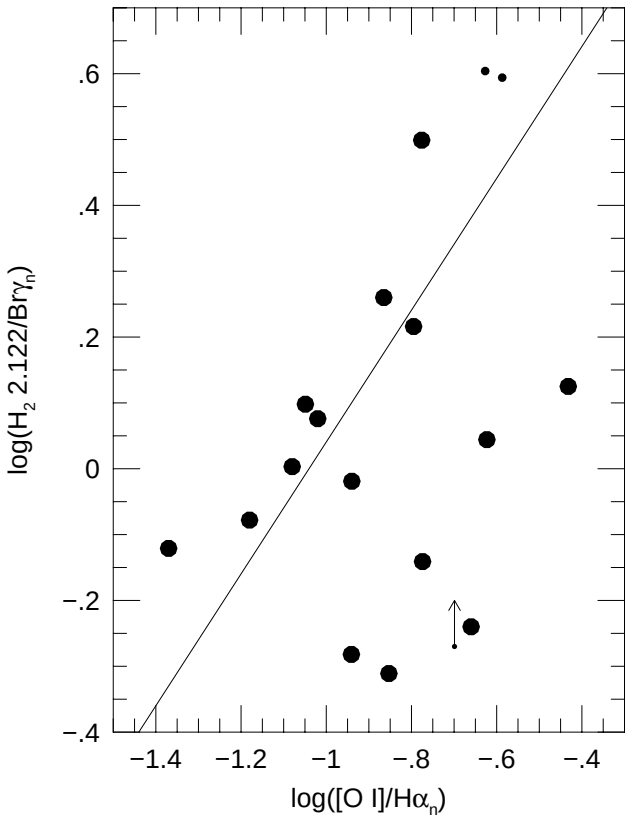

FIG. 12.—H_2 λ2.121/Brγ_n flux ratios as a function of [O I] λ6300/Hα_n flux ratios. The positions of the small symbols are uncertain. The solid line represents the predictions of the photoionization model of Lepp & McCray (1983) and Mouri et al. (1989): H_2 λ2.121/Brγ = 11 × [O I] λ6300/Hα. The data points scatter significantly around this line.

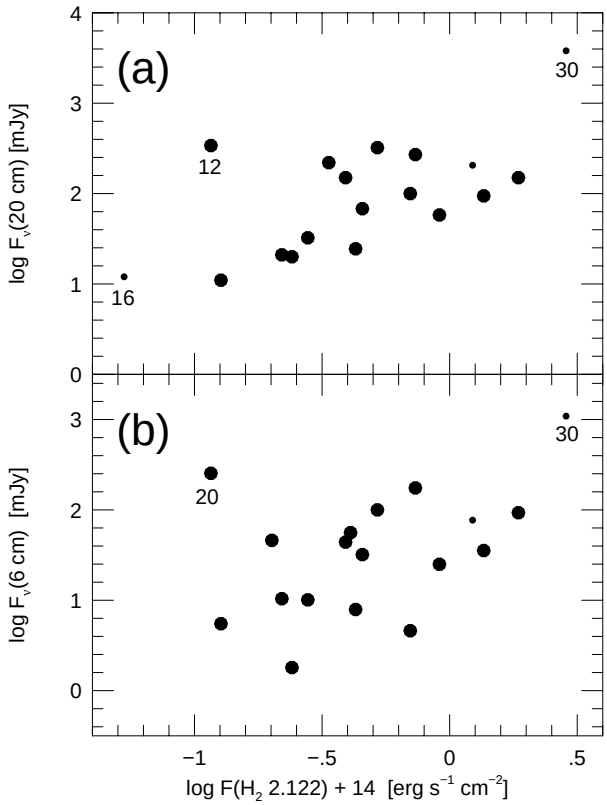

FIG. 13.—Radio fluxes as a function of H_2 λ2.121 fluxes. (*a*) 20 cm; (*b*) 6 cm. The numbers identify individual objects following the order in Table 1. The positions of the small symbols are uncertain. A weak correlation is detected in both figures.

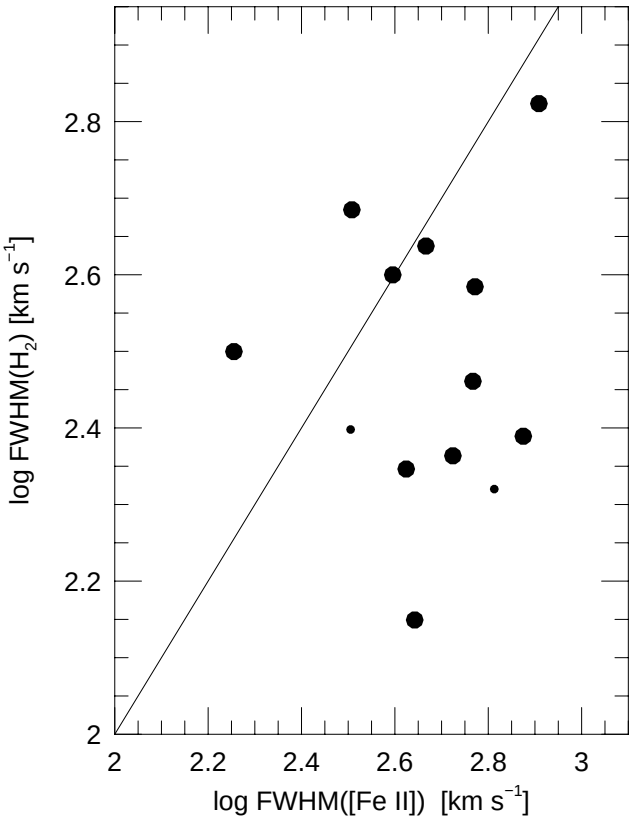

FIG. 14.—Line widths of H_2 λ2.121 as a function of the line widths of [Fe II] λ1.2567. The positions of the small symbols are uncertain. The solid line represents the equality line. No trend is observed.

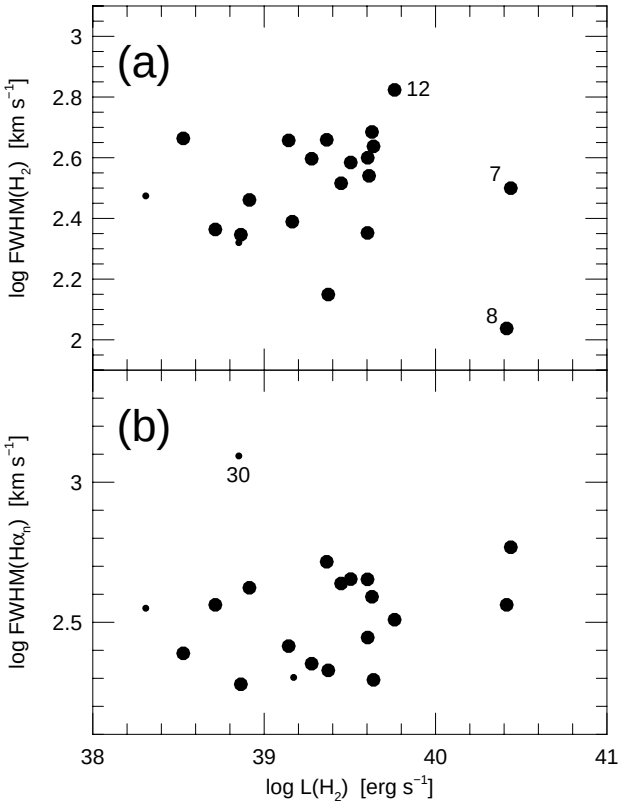

FIG. 15.—Line widths as a function of H_2 λ2.121 luminosities. (*a*) The H_2 λ2.121 line widths; (*b*) the Hα line widths. The numbers identify individual objects following the order in Table 1. The positions of the small symbols are uncertain. No significant trend is detected in our data.

replaced by the widths of Hα. This may simply reflect large variations in the environment (e.g., preshock density) or that line widths are dominated by bulk gas kinematics rather than shock details.

An important test of the shock excitation hypothesis is to verify that the mechanical energy in the purported nuclear-driven winds is sufficient to power the observed H_2 emission. Draine et al. (1983) predict a maximum efficiency of 2% for the production of H_2 1–0 $S(1)$ relative to the total available mechanical energy. For our objects, this implies a mechanical energy input ranging from $3 \times 10^6\ L_\odot$ (Akn 79 and NGC 7172) to $3 \times 10^8\ L_\odot$ (Mrk 463E and Mrk 477). These numbers should be considered lower limits to the actual values because the extinction affecting the H_2 emission was neglected. In NGC 1068, Cecil, Bland, & Tully (1990) derived a total bulk kinetic energy in the optical filaments outflowing from the nucleus of about 4×10^{53} ergs. Using a dynamical timescale of order 10^6 yr, the mechanical energy input rate in this galaxy is roughly $3 \times 10^6\ L_\odot$ and therefore appears incapable of powering all of the nuclear H_2 emission of $2 \times 10^5\ L_\odot$ in NGC 1068 at 2% efficiency (see also Rotaciuc et al. 1991).

Unfortunately, few other galaxies in the sample have been studied in sufficient detail to allow a rigorous comparison of the dynamics of the gas surrounding the nucleus with the rate required to power the observed H_2 emission through shocks. In particular, no dynamical information is available for the strongest H_2 emitters in our sample, Mrk 463E and Mrk 477. Here, we will discuss only a few additional cases. In NGC 5506, Wilson, Baldwin, & Ulvestad (1985) argue for the possible presence of a conical outflow with an outward velocity of order 300 km s^{-1}. Using their reddening-corrected Hβ luminosity of the nebula (3.4×10^{40} ergs s^{-1}) and assuming a density of order 500 cm^{-3} in the outflowing gas, a mass of $4 \times 10^5\ M_\odot$ is involved in this outflow. The mechanical energy in the outflow of NGC 5506 is thus of order a few 10^{53} ergs, i.e., similar to that of NGC 1068. The dynamical timescale for the outflow in NGC 5506 determined from the extent of the high-ionization nebula and the outflow velocity is slightly longer than that of NGC 1068. These results in turn imply a mechanical energy input rate of order 10^6 solar luminosities. In comparison, the H_2 luminosity of NGC 5506 determined by Kawara et al. (1990) requires a mechanical energy input rate of at least $10^7\ L_\odot$. These admittedly rough calculations suggest the presence of another source of H_2 emission in NGC 5506. The same problem appears to affect NGC 2110 where no evidence for any spatially resolved outflow was detected by Wilson et al. (1985; a blue wing is detected in the nuclear line profiles, however). The velocities and masses involved in the nuclear outflows of Mrk 3 (Whittle et al. 1988; Veilleux 1991c), Mrk 533 (Unger et al. 1989; Veilleux 1991c), Mrk 573 (Whittle et al. 1988; Tsvetanov & Walsh 1992), Mrk 1066 (Veilleux 1991c; Bower et al. 1995), and NGC 4388 (Corbin, Baldwin, & Wilson 1988) also seem to imply mechanical energy input rates that are too small to power all of the H_2 emission in these galaxies.

Overall, these results suggest that shock excitation by nuclear outflows is a likely mechanism for exciting the H_2 molecules in many Seyfert 2 galaxies, but that it is probably not the only source of excitation. Most likely, X-ray heating also plays an important role in producing the H_2 emission in these objects.

5. SUMMARY

A sample of 33 Seyfert 2 galaxies was observed in the J, K, and L bands to search for obscured BLRs. The presence of broad emission lines is confirmed in three objects: MCG −05-23-16, Mrk 463E, and NGC 2992. Broad-line emission may also be present in the Paβ profile of Mrk 176, Mrk 348, Mrk 1210, NGC 2110, and NGC 5728 and in the Brγ profile of Mrk 348, Mrk 477, Mrk 1210, and NGC 2110; data of higher S/N combined with careful subtraction of the stellar continuum would settle this issue. The broad-line emission that we detect is interpreted as evidence for obscured high-density BLRs based on (1) the absence of broad wings in the profile of the forbidden [Fe II] λ1.257 and H_2 λ2.122 line or (2) the lack of observational evidence for powerful high-velocity ($\sim$2000 km s^{-1}) outflows in these objects. In NGC 5506, however, *no* evidence is found for a genuine high-density BLR, but highly reddened wings that become more readily visible at longer wavelengths are detected.

Overall, these data suggest that partially obscured [A_V(IR) $\lesssim$ 10] Seyfert 1 galaxies are not uncommon. They represent perhaps as much as 25% of the Seyfert 2 galaxies in our sample. A number of these objects present small X-ray column depths. Comparisons of the (lower limits on) the broad-line extinctions in our sample galaxies with the narrow-line extinctions suggest that the obscuring material is located between the BLR and NLR. These results are consistent with the dusty wind model of Königl & Kartje (1994). The torus model of Pier & Krolik (1992b) can also explain these results if the dust content in the walls of the torus is lower, perhaps as a result of the harsh environment near the center and in the "throat" of the torus. In contrast, the thin warped disk model proposed by Sanders et al. (1989) to explain quasar spectra has difficulties accounting for many of the properties of Seyfert galaxies.

The widths of the broad components to Paβ and Brγ lie on the narrow end of the distribution for Seyfert 1 galaxies. But we must point out the difficulty to detect very broad ($\gtrsim$5000 km s^{-1}) line emission from our data. The dereddened broad Hβ luminosities predicted from the broad infrared lines are similar to the broad Hβ luminosities of normal Seyfert 1's. The ratios of the hard X-ray flux to the predicted broad Hα flux are also typical of dereddened Seyfert 1's. Only a small fraction ($\lesssim$10%) of the total broad-line flux is seen in scattered light in objects with BLR detected through both infrared spectroscopy and spectropolarimetry.

The infrared spectra of our study have also helped us constrain the origin of the [Fe II] and H_2 emission in Seyfert 2 galaxies. Our data rule out circumnuclear starbursts as the primary source of [Fe II] and H_2 emission in our objects. The [Fe II] emission is likely to originate in the cooling tails of shock fronts caused by the interaction of nuclear outflows with the ambient ISM of the host galaxies; photoionization by the nuclear continuum may also contribute to the emission. Shock excitation seems to contribute to the excitation of H_2 molecules in many Seyfert 2 galaxies but is probably not the only source of excitation. Most likely, X-ray heating also plays an important role in producing the H_2 emission in these objects. High-resolution [Fe II] and H_2 images of a large, unbiased sample of Seyfert galaxies would go a long way in removing any ambiguity.

The present sample of galaxies was biased toward objects with bright [O III] λ5007 emission. A detailed knowledge of the obscuring mass distribution in Seyfert galaxies will be possible only from the study of a large, unbiased sample of Seyfert 2 galaxies. The selection of this sample should be based on aspect-independent parameters such as the low-frequency radio emission or the far-infrared flux (see, e.g., Lawrence 1991; Mulchaey et al. 1994). The results from such a study would answer whether or not the properties of the obscured Seyfert 1 galaxies match those of normal Seyfert 1's. Seyfert 2 galaxies appear to have a higher likelihood to have companions than Seyfert 1's (see, e.g., MacKenty 1989). Tran (1995c) has argued that perturbing or merging processes may play a role in the existence and/or detection of hidden BLRs in Seyfert 2 galaxies. It will therefore be interesting to determine if the galaxies with hidden BLRs are found predominantly in multiple, interacting systems. Studies of a large sample spanning a broad range in luminosity should also clarify how the geometry of the obscuring material in active galaxies depends on the luminosity of the AGN (see, e.g., Miller & Goodrich 1990; Lawrence 1991; Mulchaey et al. 1992; Hill et al. 1996).

Substantial progress in our understanding of the mass obscuring distribution can also be made by extending the reach of our probe to larger optical depths. New probes will soon become available with the launch of the *Infrared Space Observatory* (*ISO*) and the *Advanced X-ray Astronomical Facility* (*AXAF*). In particular, observations of the profiles of the high-J $^{12}C^{16}O$ and medium-J $^{13}C^{16}O$, $^{12}C^{18}O$, and $^{12}C^{16}O$ rotational lines should provide a direct view of the molecular gas near the AGNs (Krolik & Lepp 1989). VLBI observations of maser emission from active galaxies are also proving to be a powerful technique to probe the accretion disk in these objects at subparsec scales (see, e.g., Greenhill et al. 1995).

We thank the anonymous referee and the Scientific Editor, S. Willner, for several suggestions that improved this paper. Parts of this work have been supported by NASA through grant HF-1039.01-92A awarded by the Space Telescope Science Institute which is operated by the AURA, Inc. for NASA under contract NAS 5-26555 (S. V.) and by the NSF through grant AST 91-21889 (R. W. G.). This research has made use of the NASA/IPAC Extragalactic Database (NED) which is operated by the Jet Propulsion Laboratory, California Institute of Technology, under contract with NASA.

APPENDIX A

NOTES ON INDIVIDUAL OBJECTS

In this Appendix, we discuss the emission-line properties of each object, with particular emphasis on the presence or absence of broad components in the profiles of the infrared hydrogen recombination lines. In the cases where no positive detection of broad emission is reported, we often give very conservative upper limits to the broad-line fluxes. These broad-line fluxes were determined by fitting the maximum broad Gaussian consistent with the data.

A1. MCG −05-23-16 = A0945−30

The high-resolution spectrum of MCG −05-23-16 from Paper I clearly shows a strong broad Paβ line with FWHM $\approx$ 2490 km s^{-1} beneath a weaker narrow component, confirming the earlier results of Blanco et al. (1990). The presence of this broad-line emission is also evident in the profile of Brγ in our new K-band data of this galaxy (Fig. 1*a*). This broad component dominates the Brγ profile, which makes it impossible to measure the contribution from the narrow-line region. As a consequence, the broad-line Brγ flux listed in Table 3 should be considered an upper limit to the actual broad-line flux, and the width of this broad component, a lower limit to the actual line width. An estimate of the narrow-line Brγ flux can be derived using the narrow Hβ, Hα, and Paβ fluxes and the narrow-line extinctions determined from these fluxes: $F(\mathrm{Br}\gamma_n) = 0.7 \times 10^{-14}$ ergs s^{-1} cm^{-2}, consistent with being a minor contributor to the total observed Brγ flux.

The presence of any broad component to the Balmer lines in MCG −05-23-16 is hotly debated (see discussion in Paper I). The results are extremely sensitive to the template profiles used to deblend the Hα + [N II] complex. We consider the value obtained by Durret & Bergeron (1988; $F[\mathrm{H}\alpha_b] = 18 \times 10^{-14}$ ergs s^{-1} cm^{-2}) a generous upper limit to broad Hα. Using this measurement, $E(B-V)_b > 2.3$ based on Paβ_b/Hα_b and $E(B-V)_b > 1.9$ based on Brγ_b/Hα_b. Note, however, that Paβ_b/Brγ_b implies $E(B-V)_b = 0.6$, a value that is inconsistent with these upper limits. This inconsistency is difficult to explain. A conservatively high value of $E(B-V)_b \gtrsim 2$ is adopted.

A2. MRK 3

Miller & Goodrich (1990) and Tran (1995a) detected a BLR in Mrk 3 using spectropolarimetry, but low-resolution J-band spectra do not reveal any obvious BLR at Paβ (Paper I). The high declination of Mrk 3 prevented us from obtaining high-resolution UKIRT data of this galaxy.

A3. MRK 78

Mrk 78 lies above UKIRT's upper limit on declination. Our low-resolution J-band spectra obtained on the UH 88 inch (2.24 m) telescope did not reveal any BLR at Paβ (Paper I). No BLR was detected in Mrk 78 from spectropolarimetry (Miller & Goodrich 1990; Tran 1995a).

A4. MRK 176

Our J-band spectrum of Mrk 176 shows a weak narrow Paβ line lying on a broad pedestal interpreted in Paper I as either an undulation in the underlying continuum or a broad Paβ emission feature with FWHM $\approx$ 1500 km s^{-1}. Ruiz et al. (1994) confirmed the presence of this broad feature in Paβ and detected a similar feature in He I λ10830. Figure 1*b* presents our new K-band spectrum of this object. Disappointingly, the K-band spectrum of this object is nearly featureless: H_2 2.121 μm is barely detected, and we were able to derive only an upper limit on the intensity of Brγ. If the broad wings of Paβ reflect the presence of a BLR, $F(\mathrm{Pa}\beta_b) \approx 1 \times 10^{-14}$ ergs s^{-1} cm^{-2}. Assuming that a BLR with one-fifth the intensity of the observed Hα emission would have been detected, $E(B-V)_b \gtrsim 2$.

A5. MRK 266SW = NGC 5256SW

Kay (1994) tentatively reported the detection of a broad Hα line in the polarized light of Mrk 266SW. No broad Paβ was detected in this galaxy (Paper I), nor is there any evidence for broad wings to Brγ in the new spectrum (Fig. 1*c*). We derive upper limits on the Paβ and Brγ flux produced from the BLR of this galaxy of about 1.0 and 0.1 $\times 10^{-14}$ ergs s^{-1} cm^{-2}, respectively.

The reddening derived from the narrow-line ratio Paβ_n/Hα_n differs significantly from the values based on Brγ_n/Hα_n or the Balmer decrement. This apparent discrepancy may be due to differential slit losses associated with the extended nature of the line-emitting region in this galaxy(Mazzarella et al. 1988). Slight changes in the seeing and positioning of the slit can cause variations in the flux entering the spectrograph aperture. The differences in the profiles of [Fe II] 1.2567 μm, Paβ, H_2 2.121 μm, Brγ, and [O III] λ5007 may also be explained in that way. The obvious blue wing in the profile of [O III] λ5007 (Vrtilek & Carleton 1985) is not visible in any of the infrared line profiles. Significant structure was detected in the red wing of Paβ (Paper I), but the S/N of the K-band data is insufficient to confirm the presence of this feature in Brγ.

A6. MRK 266NE = NGC 5256NE

There is no evidence of a BLR in the Paβ profile of this LINER galaxy (Paper I). No attempt was made to acquire a K-band spectrum of this object.

A7. MRK 463E

Mrk 463E is a "warm" ultraluminous (log $[L/L_\odot] = 12.03$) *IRAS* galaxy with a Seyfert 2 optical spectrum (see, e.g., Sanders et al. 1988). Near-infrared spectra of this object reveal a broad component to the recombination lines of hydrogen and helium (Blanco et al. 1990; Paper I; Ruiz et al. 1994). A broad Paβ component with FWHM $\approx$ 1810 km s^{-1} was clearly detected in our J-band spectrum of Mrk 463E (Paper I). Spectropolarimetric observations by Miller & Goodrich (1990) and Tran (1995a) also reveal a hidden BLR, seen in scattered, polarized light. The ratio of Paβ_b emission to scattered Hα_b emission is $\sim$2, more than an order of magnitude larger than the value predicted from Case B recombination (and considerably larger than the value originally quoted in Paper I).

The new K-band spectrum of Mrk 463E (Fig. 1*d*) also suggests the presence of a broad component to Brγ. The data are not as convincing as the Paβ data because the line-to-continuum contrast in this galaxy is considerably lower at K than at J and because a strong sky line at 2.281 μm is contaminating the red wing of Brγ. Once again, the ratio of Brγ_b emission to scattered Hα_b emission is an order of magnitude above the Case B value. Making the rather safe assumption that a BLR with one-fifth

the intensity of the observed Hα emission would have been detected in previous optical spectra, we derive a lower limit to the color excess in the BLR based on $Pa\beta_b/H\alpha_n$ and $Br\gamma/H\alpha_n$: $E(B-V)_b > 3.2$ and 1.9, respectively. The value derived from $Pa\beta_b$ is considered more reliable.

A8. MRK 477 = I Zw 92

Mrk 477 is another Seyfert 2 galaxy with polarized broad Hα (Tran et al. 1992; Tran 1995a). No obvious broad Paβ emission was detected in our *J*-band spectra (Paper I), although the relatively low resolution of the spectra undoubtedly hampered our ability to detect a broad feature with FWHM $\gtrsim 3000$ km s^{-1} (Tran 1995a).

The new *K*-band spectrum of Mrk 477, shown in Figure 1*e*, presents relatively strong, narrow H_2 2.121 μm and Brγ features. An apparent broad component to Brγ is marginally detected. If real, the broad $Br\gamma_b$ emission is about 6 times larger than that predicted using Case B recombination and the scattered broad emission of Tran (1995a, 1995c). The presence of broad Brγ emission combined with the lack of any broad Hα or Paβ emission at the level of at least one-fifth the intensity of the narrow line implies that $E(B-V)_b \gtrsim 0.8$ or $\gtrsim 1.7$, respectively. These values are smaller than the lower limit on $E(B-V)_b$ implied by the absence of broad Paβ [A_V(BLR) $\gtrsim 11$]. Data of higher S/N will be needed to confirm the presence of broad Brγ.

A9. MRK 1388

No BLR was detected in the Paβ profile of this unusually high ionization Seyfert 2 galaxy (Paper I). No new *K*-band spectrum was obtained of this galaxy.

A10. NGC 2992 = MCG −02-25-14

The optical spectrum of the narrow-line X-ray galaxy NGC 2992 is fairly typical of that of a normal Seyfert 2 galaxy with the exception of a possible weak broad component to Hα (Shuder 1980; Véron et al. 1980). In contrast, broad emission is clearly observed in the profile of Paβ (Paper I; Rix et al. 1990). The *K*-band spectrum of NGC 2992 is characterized by weak Brγ emission but relatively strong H_2 emission (Fig. 1*f*). There is a slight excess of broad emission with FWHM ≈ 4000 km s^{-1} on each side of narrow Brγ, but it may simply reflect structure in the underlying stellar continuum or small errors in the continuum calibration. Consequently, the flux of $Br\gamma_b$ listed in Table 3 should be considered an upper limit.

A direct estimate of the reddening in the BLR of NGC 2992 can be derived from the intensity of the broad line at Paβ and Brγ: assuming Case B recombination, $E(B-V)_b = 2.1$. The broad Hα fluxes measured by Shuder (1980) or Véron et al. (1980) can also be used to determine the extinction toward the BLR. Using the value of Véron et al. (1980), $E(B-V)_b \approx 2.6$ from $Pa\beta/H\alpha$ and 2.5 from $Br\gamma/H\alpha$, while the $H\alpha_b$ flux of Shuder (1980) implies $E(B-V)_b \approx 0.9$ from $Pa\beta/H\alpha$ and 1.2 from $Br\gamma/H\alpha$.

The color excesses derived from the narrow lines of NGC 2992 show a tendency to *decrease* with wavelengths. This result is difficult to explain unless differential slit loss, seeing, and guiding effects are affecting the data on this object. This may be the case since the line-emitting region in NGC 2992 is known to be extended and complex (Wehrle & Morris 1988).

A11. NGC 3081 = IC 2529

The *J*-band spectrum of NGC 3081 shows faint narrow Paβ and [Fe II] λ1.2567 emission lying on top of a strong stellar continuum (Paper I). Detection of a broad component to Paβ is therefore difficult unless the stellar continuum is very carefully removed from the data. For this reason, no attempt was made to observe NGC 3081 in the *K* band.

A12. NGC 4388

There is no evidence for broad Paβ emission in NGC 4388 (Blanco et al. 1990; Paper I). This result was recently confirmed by Ruiz et al. (1994). We now report on new attempts to detect a broad line in Brγ and Brα. The new spectra show no obvious sign of a broad component to any of these lines (Figs. 1*g* and 1*h*). Since both the line-to-continuum contrast and S/N of the new data are slightly lower than in the *J*-band data presented in Paper I, the constraints on broad Brγ and broad Brα are relatively weaker than that on broad Paβ: $F(Pa\beta_b) < 1.5 \times 10^{-14}$ ergs s^{-1} cm^{-2}, $F(Br\gamma_b) < 1.3 \times 10^{-14}$ ergs s^{-1} cm^{-2}, $F(Br\alpha_b) < 7.6 \times 10^{-14}$ ergs s^{-1} cm^{-2}. Our failure to detect broad-line emission from the nucleus of this galaxy is surprising in view of the reported off-nuclear broad Hα in this galaxy (Shields & Filippenko 1988).

With the exception of the color excess derived from $Br\gamma_n/H\alpha_n$, there is a general tendency for the amount of reddening derived from the narrow lines in NGC 4388 to increase toward longer wavelengths (see Table 3). This suggests the presence of an obscured source of narrow-line emission only visible at infrared wavelengths.

A13. NGC 5252

The Paβ emission in NGC 5252 is very faint, and the *J*-band continuum appears dominated by stellar light (Paper I). No strong statement could be made in Paper I on the presence of an obscured BLR in this galaxy. Our *K*-band spectrum of NGC 5252 is nearly featureless (Fig. 1*i*); Brγ is barely detected in this spectrum. The optical fluxes listed in Table 3 were derived from spectra obtained with an aperture (8″) that is considerably larger than that of the infrared data. The color excesses listed in Table 3 and derived from the ratios of the infrared lines to the Hβ flux are therefore lower limits to the actual reddening. For instance, if the Hβ flux is divided by the ratio of the aperture sizes (i.e., assuming that the Hβ flux is uniformly distributed inside of the large optical aperture), $E(B-V)_n \approx 1.1$ from the Paβ flux and $E(B-V)_n \approx 0.4$ from the estimated Brγ flux.

A14. NGC 5506

In Paper I, we argued against the presence of genuine broad Paβ emission in NGC 5506 based on the fact that the Paβ profile is continuous and has the same shape as the nearby [Fe II] λ1.2567, a forbidden line that cannot be produced in the high-density BLR. However, the NLR profiles were found to become broader at longer wavelengths, which suggests that the

wing emission is highly reddened. We therefore argued that the "broad" Paβ line reported by Blanco et al. (1990) and Rix et al. (1990) (and, more recently, by Ruiz et al. 1994) corresponds to the strong, highly reddened emission in the wings of this profile.

New spectra centered on Brγ and Brα were obtained of NGC 5506; they are shown in Figures 1*j* and 1*k*. The lower S/N and absence of strong forbidden lines in these data prevent us from making strong statements on the presence of BLR emission in Brγ and Brα. The profile of Brγ is similar to that of Paβ (Paper I): it presents a narrow core superposed on a broad base. This profile is affected by sky line residuals at 2.188 and 2.206 μm, and structure in the underlying stellar continuum may also be responsible for the break around 2.16 μm in the continuum of NGC 5506.

The line fluxes and widths listed in Tables 3 and 4 were derived by fitting the sum of a Gaussian and a Lorentzian, both with the same FWHM and the same peak strength. This profile was shown in Paper I to fit the Paβ profile very well; Brγ and Brα are also well fitted by this hybrid profile. The fluxes in the tables are significantly larger than those obtained by Moorwood & Oliva (1988) and Kawara et al. (1988). A similar result is found when comparing our Paβ and [Fe II] λ1.2567 fluxes to those of Blanco et al. (1990) and Rix et al. (1990). The origin of this discrepancy is unclear, but it may be due at least in part to differences in the placement of the slit. All of our spectra were centered on the *infrared* peak, while the slit was centered on the *optical* peak in the other studies. In an edge-on galaxy like NGC 5506, where the nucleus is undoubtedly obscured by dust in the galaxy disk, the position of the optical nucleus can differ by a few arcseconds from that of the infrared nucleus (see, e.g., Veilleux et al. 1994). This may account for the discrepancy between our data and those obtained through relatively small apertures (Blanco et al. 1990 and Rix et al. 1990) but has difficulties explaining the difference between our results and those of Moorwood & Oliva (1988) and Kawara et al. (1989) who used apertures of $6'' \times 6''$ and $10''.3 \times 20''.7$, respectively.

The color excesses derived from the fluxes in Tables 3 and 4 are significantly larger than the value derived from the Balmer decrement. There are relatively little variations in the colors excesses derived from Paβ, Brγ, and Brα. Once again, this result suggests that an unreddened source dominates the optical line emission in NGC 5506, while the infrared line emission is produced in a stronger, reddened source but not in what would be termed a BLR (see discussion in Paper I).

A15. NGC 5728 = MCG −03-37-5

Based on a *J*-band spectrum of rather low S/N, NGC 5728 was classified in Paper I as a possible candidate for an obscured Seyfert 1 galaxy. Unfortunately, the Brγ feature in our new *K*-band spectrum is too faint to clarify the situation (Fig. 1*l*). It is not clear either why the color excess derived from the narrow-line Balmer decrement is larger than the value derived from $\mathrm{Pa}\beta_n/\mathrm{H}\alpha_n$, which itself is larger than the value derived from $\mathrm{Br}\gamma_n/\mathrm{H}\alpha_n$.

A16. AKN 79

Akn 79 is the active galaxy with the weakest optical emission lines in our sample (Shuder & Osterbrock 1981; Dahari & De Robertis 1988). High-resolution spectroscopy of these lines reveals the presence of a significant blue wing (see, e.g., Vrtilek & Carleton 1985). Figure 2*a* shows the *K*-band spectrum of this galaxy. Very few emission lines are visible. H_2 λ2.121 is present at 2.16 μm, and the feature near 2.265 μm may correspond to H_2 λ2.223. An upper limit of 1×10^{-15} ergs s^{-1} cm^{-2} was derived on the total flux of Brγ.

A17. ESO 428-G14 = M4-1 = MCG −5-18-2

ESO 428-G14 was first classified as a planetary nebula, PK 241 − 7°1 (Perek & Kohoutek 1967); subsequent spectroscopy revealed that it was in fact a galaxy with the emission-line properties of a Seyfert 2 (Bergvall, Johansson, & Olofsson 1986). Direct imaging and long-slit spectroscopy by Wilson & Baldwin (1989) have shown that the nuclear regions of ESO 428-G14 contain an extended ($\sim$1 kpc) high-excitation nebulosity that is well aligned with the curved, jetlike nonthermal radio source (Ulvestad & Wilson 1989). The spectrum around Paβ is displayed in Figure 2*b*. The profile of Paβ is narrower than the equally strong [Fe II] λ1.2567. Excess emission in the blue wing of Paβ is attributed to He I λ1.27887. Broad Paβ with FWHM $\approx$ 1400 km s^{-1} cannot contribute more than 4.7×10^{-14} ergs s^{-1} cm^{-2}.

The fluxes derived by Bergvall et al. (1986) were used to calculate the narrow-line color excesses listed in Table 3. These fluxes were obtained through a $4'' \times 4''$ aperture, while our infrared fluxes were determined from a spectrum that was extracted from a $3'' \times 3''$ region.

A18. IC 5135 = NGC 7130

IC 5135 was originally identified as a Seyfert 2 galaxy by Phillips, Charles, & Baldwin (1983). More recently, Shields & Filippenko (1990) studied its optical emission-line spectrum in detail and concluded that a circumnuclear starburst is also present in this object. No spectrum was obtained in the *J* band. The line emission from Brγ and H_2 2.121 μm dominates the *K*-band spectrum (Fig. 2*c*). Both lines have similar widths, and neither shows any obvious broad wings at low intensity levels. Any broad (FWHM $\approx$ 2600 km s^{-1}) emission at Brγ must be weaker than about 3×10^{-15} ergs s^{-1} cm^{-2}. A number of other features may be identified in the spectrum. The line at 2.094 μm is redshifted He I λ2.058, while the weaker features at 2.26 μm and 2.110 μm probably correspond to H_2 λ2.223 and H_2 λ2.073, respectively.

A19. MRK 1 = NGC 449

The optical spectrum of Mrk 1 was first studied in detail by Koski (1978). The emission-line properties of this galaxy are typical of active galaxies photoionized by a hard continuum source (see, e.g., Koski 1978; Osterbrock, Tran, & Veilleux 1992). The profiles of the emission lines at optical wavelengths present a distinct blue asymmetry and have FWHM $\approx$ 500 km $^{-1}$ (see, e.g., Busko & Steiner 1989, 1992; De Robertis & Shaw 1990). Interestingly, this profile asymmetry is not visible in the

profiles of Brγ and H_2 λ2.121, the two strongest lines in the K-band spectrum of Mrk 1 (Fig. 2*d*). The profile of Brγ appears only marginally broader than that of H_2 λ2.121. There is therefore no strong evidence for an obscured BLR in this galaxy. We put a conservatively high upper limit of 2×10^{-15} ergs s^{-1} cm^{-2} on the flux from broad (FWHM $\approx$ 2500 km s^{-1}) Brγ. Mrk 1 is one of the few galaxies in our sample in which both H_2 λ2.223 and He I λ2.073 are sufficiently strong to allow the fluxes of these lines to be measured accurately.

A20. MRK 348 = NGC 262

Mrk 348 is a Seyfert 2 galaxy that exhibits very broad Hα in polarized light (FWHM = 8400 km s^{-1}; Miller & Goodrich 1990; Tran 1995a). The existence of this broad Hα emission was first suspected by De Robertis & Osterbrock (1986). Ruiz et al. (1994) recently reported the detection of faint blue-wing emission with FWHM $\approx$ 900–1600 km s^{-1} in the profiles of He I λ1.083 and Paβ. Our J-band spectrum confirms the presence of this excess of emission in the blue wing of Paβ (Fig. 2*e*). This excess emission is not visible in [Fe II] λ1.2567 or fourth-order [S III] λ0.9532. Unfortunately, it is not clear whether this excess emission corresponds to broad Paβ emission or represents contamination by He I λ1.27887. The K-band spectrum does not clarify the situation (Fig. 2*f*). The profile of Brγ appears broader at the base than that of H_2 λ2.121, but structure in the K-band continuum prevents us from making a firm statement. A two-Gaussian decomposition of the Paβ and Brγ profiles provides upper limits to the broad-line flux in this galaxy: $F(\mathrm{Pa}\beta_b) \lesssim 1 \times 10^{-14}$ ergs s^{-1} cm^{-2}, $F(\mathrm{Br}\gamma_b) \lesssim 7 \times 10^{-16}$ ergs s^{-1} cm^{-2}, FWHM(Paβ_b) $\approx$ 1,850 km s^{-1}, and FWHM(Brγ_b) $\approx$ 2500 km s^{-1}. Data of higher S/N will be needed to better assess the importance and origin of this excess emission.

A21. MRK 403

The optical spectrum of Mrk 403 has been studied by Osterbrock & Dahari (1983) and Veilleux & Osterbrock (1987). The most stunning feature of the J-band spectrum (Fig. 2*g*) is the near absence of [Fe II] λ1.2567: $F([\mathrm{Fe\ II}])/F(\mathrm{Pa}\beta) \lesssim 0.34$. Emission from He I λ1.27887 seems to contaminate the blue wing of Paβ. The structure in the continuum near Paβ makes the placement of the continuum difficult. No evidence is seen for broad Paβ at a flux level of more than 8×10^{-15} ergs s^{-1} cm^{-2} (FWHM $\approx$ 3800 km s^{-1}).

A22. MRK 533 = NGC 7674

Spectropolarimetry of NGC 7674 reveals broad Hα emission with FWHM = 2830 km s^{-1} in polarized light (Miller & Goodrich 1990; Tran 1995a). The optical emission lines of this object are well known to present remarkable blue wings extending up to velocities of 2000 km s^{-1} with respect to the peak velocity (see, e.g., Veilleux 1991a). Our infrared spectra of this object are presented in Figures 2*h* and 2*i*. The profiles of both Paβ and Brγ are characterized by a narrow core superposed on a broad base blueshifted with respect to the narrow core. Ruiz et al. (1994) arrived at a qualitatively similar result for He I λ1.083 and Paβ.

To disentangle the true origin of the broad base in the infrared line profiles, it is important to note that the profiles of Paβ and Brγ are similar to that of [O III] λ5007 (Veilleux 1991a, 1991b). These results suggest that the broad component in the profiles of Paβ and Brγ represents emission from a NLR rather than from a genuine high-density BLR (in which [O III] λ5007 is collisionally de-excited). Veilleux (1991c) has argued that the spectacular blue wing in the line profiles of Mrk 533 is produced by gas of high ionization. This explanation is also consistent with the fact that the extended blue wing is not apparent in the profiles of the low-excitation lines [Fe II] λ1.2567 and H_2 λ2.121.

The fluxes listed in Table 3 were derived by fitting the profiles with the sum of a Gaussian and a Lorentzian, both with the same FWHM and the same peak strength. The NLR reddenings determined from Paβ/Hβ and Brγ/Hβ are larger than the reddening determined from the Balmer decrement, perhaps a sign that the infrared lines are probing deeper column depths than the Balmer lines.

A23. MRK 573 = UM 363

Mrk 573 is a high-ionization Seyfert 2 galaxy which shows strong evidence for a biconical radiation field (see, e.g., Tsvetanov & Walsh 1992; Pogge & De Robertis 1993). The extended narrow-line emission of Mrk 573 is roughly aligned with the axis of the triple source at radio wavelengths (P.A. $\approx$ 124°; Ulvestad & Wilson 1984a). A BLR was tentatively detected in the polarized light of Mrk 573 (Kay 1994). The Paβ profile (Fig. 2*j*) is very similar to that of [Fe II] λ1.2567, implying $F(\mathrm{Pa}\beta_b) < 5 \times 10^{-15}$ ergs s^{-1} cm^{-2}. He I λ1.27887 and λ1.2528 are detected blueward of Paβ and [Fe II], respectively. The K-band spectrum of Mrk 573 (Fig. 2*k*) is characterized by a strong stellar continuum and relatively faint emission from Brγ and H_2 λ2.121. Both He I λ2.058 and H_2 λ2.223 also appear to be present in the spectrum. The flux of Brγ_b is less than 1×10^{-15} ergs s^{-1} cm^{-2}. A spectrum of higher S/N will be needed to subtract accurately the underlying stellar continuum from the spectrum of Mrk 573 and to put stronger constraints on the contribution of Brγ_b.

A24. MRK 622

Mrk 622 is a Seyfert 2 galaxy whose optical emission-line properties have been studied in detail by Shuder & Osterbrock (1981). Figure 2*l* displays the spectrum of Mrk 622 near Paβ. The spectrum around 1.308 μm has been interpolated to get rid of a strong cosmic ray. There is no obvious sign for a broad component to Paβ: $F(\mathrm{Pa}\beta_b) < 1.4 \times 10^{-14}$ ergs s^{-1} cm^{-2} with FWHM $\approx$ 2700 km s^{-1}. The width of Paβ is slightly smaller than that of [Fe II] λ1.2567. No K-band spectrum was obtained of this galaxy.

A25. MRK 917 = MCG +05-53-09

The optical and ultraviolet spectrum of Mrk 917 is indicative of photoionization by a hard power-law source (Ferland & Osterbrock 1986; Veilleux & Osterbrock 1987; Osterbrock et al. 1992). Durret (1994) detected ionized gas in this galaxy over 15″ (10.5 kpc for a distance of 145 Mpc). The *K*-band spectrum of Mrk 917 reveals relatively strong Brγ and H_2 λ2.121 lines of nearly equal strengths (Fig. 2*m*). There is no evidence for any broad emission at Brγ; in fact, the H_2 line appears slightly broader than Brγ. We derive $F(\mathrm{Br}\gamma_b) < 1.8 \times 10^{-15}$ ergs s^{-1} cm^{-2}. The He I λ2.058 and H_2 λ2.223 lines are barely detected in our spectrum.

A26. MRK 1066

Mrk 1066 is a Seyfert 2 galaxy with strong, narrow emission lines (Goodrich & Osterbrock 1983; Veilleux & Osterbrock 1987; Veilleux 1991a). The radio map of Ulvestad & Wilson (1989) shows a linear, probably triple, source extending 2.″8 along P.A. 134° $\pm$ 4°. A direct relationship seems to exist between the radio structure and the optical line emission in Mrk 1066 (Haniff, Wilson, & Ward 1988; Veilleux 1991c). Recent *HST* results indicate that the [O III]–emitting gas is concentrated into a bright "jetlike" structure that coincides with the northwest radio jet (Bower et al. 1995). No hidden BLR was detected from spectropolarimetry (Miller & Goodrich 1990). The *J*-band spectrum of Mrk 1066 shows strong [Fe II] λ1.2567 and Paβ (Fig. 2*n*). Both profiles have roughly the same widths as the optical lines. Weak excess emission is seen in the blue wing of both lines. Some of the excess in Paβ is almost certainly due to He I λ1.27887.

The *K*-band spectrum of Mrk 1066 harbors strong, symmetric lines from H_2 λ2.121 and Brγ (Fig. 2*o*). He I λ2.058 is also clearly present, while H_2 λ2.223 is a marginal detection. The high quality of our infrared spectra allows us to put stringent constraints on the flux from broad Paβ and Brγ: $F(\mathrm{Pa}\beta_b) < 4.8 \times 10^{-14}$ ergs s^{-1} cm^{-2} (FWHM $\approx$ 1500 km s^{-1}) and $F(\mathrm{Br}\gamma_b) < 3.5 \times 10^{-15}$ ergs s^{-1} cm^{-2} (FWHM $\approx$ 2850 km s^{-1}).

A27. MRK 1073 = MCG +7-7-37

The optical spectrum of Mrk 1073 presents strong, narrow but slightly blue asymmetric emission lines with FWHM $\approx$ 250 km s^{-1} (Veilleux 1991a, 1991b). Low-ionization substructure in the core of these lines has been attributed to a separate line-emitting region located $\sim$4″ from the nucleus (Veilleux 1991c). The spectrum of Mrk 1073 around Paβ is shown in Figure 2*p*. The Paβ profile shows a broad blue wing that does not seem to be present in the profile of [Fe II] λ1.2567. Note, however, that [Fe II] lies near the edge of our spectrum, which makes its blue wing less reliable. Moreover, contamination by He I λ1.27887 is likely to contribute to the blue excess in Paβ. Excess emission is also visible in the red wing of Paβ but at a much lower intensity level.

Assuming that all of the blue and red wing emission in Paβ is produced by an obscured BLR, $F(\mathrm{Pa}\beta_b) \approx 3.7 \times 10^{-14}$ ergs s^{-1} cm^{-2} and FWHM(Paβ_b) $\approx$ 1600 km s^{-1}. These results would imply $E(B-V)_b \gtrsim 1.8$, under the assumption that a broad Hα component with at least one-fifth the strength of the observed narrow component would have been detected in the published optical spectra. Perhaps the best test for the presence of an obscured BLR in Mrk 1073 is to search for broad Brγ. There is very little evidence for a BLR in the *K*-band spectrum of Mrk 1073 (Fig. 2*q*). The profile of Brγ is slightly broader than that of H_2 λ2.121, but the blue excess that was present in Paβ is absent in Brγ. We derive $F(\mathrm{Br}\gamma_b) < 2 \times 10^{-15}$ ergs s^{-1} cm^{-2} with FWHM $\approx$ 3700 km s^{-1}. This flux is less than the value expected from Case B recombination using the broad Paβ flux assumed above. These results imply that only a fraction of the wing emission in Paβ can possibly be produced in a genuine BLR.

A28. MRK 1157 = NGC 591

Mrk 1157 is an early-type barred spiral galaxy with Hα extending over $\sim$30″ in the east-west direction (Haniff et al. 1988). In contrast, the bulk of the [O III] λ5007 emission is produced in a region centered on the continuum nucleus that is only marginally resolved in the northwest-southeast direction. This position angle coincides with that of the linear radio double observed by Ulvestad & Wilson (1989; PA = 152°). The optical emission-line profiles in the nucleus of Mrk 1157 present a very high degree of symmetry (Veilleux 1991a), contrary to what is generally observed in Seyfert 2 galaxies. Miller & Goodrich (1990) did not detect any BLR in the polarized light of Mrk 1157. The *K*-band spectrum of Mrk 1157 is presented in Figure 2*r*. No data were obtained in the *J* band. Strong H_2 line emission is observed: $F(H_2\ \lambda2.121)/F(\mathrm{Br}\gamma) \approx 1.8$. H_2 λ2.223 and He I λ2.058 are also clearly present in the spectrum. The dominance of H_2 is not surprising since Mrk 1157 is one of the few Seyfert 2 galaxies that have been detected in CO (see, e.g., Taniguchi et al. 1990). Comparison of the profiles of Brγ and H_2 λ2.121 indicates that a broad component to Brγ cannot contribute more than 1.8×10^{-15} ergs s^{-1} cm^{-2} (FWHM $\approx$ 3800 km s^{-1}) to the total Brγ emission.

A29. MRK 1210

Tran et al. (1992) and Tran (1995a) reported the detection of a BLR in the polarized light of Mrk 1210. The broad polarized Hα emission has a flux of about 6×10^{-15} ergs s^{-1} cm^{-2} and a width of 2380 km s^{-1}. The *J*-band and *K*-band spectra are presented in Figures 2*s* and 2*t*. The Paβ profile is characterized by a strong narrow component on top of a broad base with FWHM $\approx$ 1600 km s^{-1}. A comparison of the Paβ profile with that of [Fe II] λ2.1567 suggests that at least part of this broad emission is also present in [Fe II] and therefore is not produced in a genuine high-density BLR. The profile of Brγ also presents a narrow core on top of a broad base and appears considerably broader than H_2 2.121 μm. However, the measured strength and width of the broad component is uncertain due to noise in the spectrum. Consequently, the broad-line fluxes listed in columns (5) and (11) of Table 3 should be considered generous upper limits to the actual values. Taken at face value, the strengths of the broad-line emission at Paβ and Brγ imply flux ratios relative to broad scattered Hα more than an order of

magnitude larger than Case B recombination. The possible presence of a broad component to Paβ and Brγ and the absence of broad Hα would also imply $E(B-V)_b \gtrsim 1.6$ and 1.1, respectively

Lowering the contribution of the BLR to the infrared lines would increase the color excesses determined from *narrow* Paβ and Brγ, and this may explain why the reddenings determined from Paβ/Hα and Brγ/Hα are smaller than the values determined from the Balmer decrement. Differential slit loss may also affect these numbers since the optical data of Terlevich et al. (1991) were obtained through a $2'' \times 4''$ aperture, while our J-band and K-band spectra were extracted from $3'' \times 6''$ and $1''.5 \times 1''.5$ regions, respectively.

A30. NGC 1068

NGC 1068 is the archetypical example of Seyfert 2 galaxies with hidden BLR visible in scattered, polarized light (see, e.g., Antonucci & Miller 1985; Bailey et al. 1988; Miller, Goodrich, & Mathews 1991). The polarized Hβ and Hα emission lines exhibit a profile with FWHM $\approx$ 4500 km s^{-1}. A number of attempts have already been made to detect a broad line in Brγ (Thompson, Lebofsky, & Rieke 1978; Hall et al. 1981; DePoy 1987), Brα, and Pfβ λ4.6525 (DePoy 1987). None of these studies have been successful in detecting infrared emission lines that are broader than the unpolarized optical lines (FWHM $\approx$ 1000 km s^{-1}; Cecil et al. 1990; Veilleux 1991b). Our own data are displayed in Figure 2*u*. No obvious broad-line emission is detected at Brγ. The Brγ flux is similar to that determined by Kawara et al. (1989) and Goldader et al. (1997). The H_2 λ2.121 feature is visible in our spectrum but at a considerably lower level than the value measured by Moorwood & Oliva (1990) and Goldader et al. (1997). Since the H_2 emission is extended in this galaxy (Blietz et al. 1994), differences in the aperture sizes and centering may explain some of this discrepancy.

Our K-band spectrum illustrates the difficulty in trying to detect a broad component to the infrared recombination lines of NGC 1068. The profile of Brγ is strongly affected by the underlying stellar and dust continuum that dominates the line emission by nearly 2 orders of magnitude. An attempt was made to subtract the stellar continuum from these data using a spectrum of the elliptical galaxy NGC 1700 obtained under identical conditions. The stellar continuum of NGC 1700 was found to be a rather poor match to that of NGC 1068.

Failure to detect the BLR at infrared wavelengths implies large extinctions, perhaps A_v(BLR) $\gtrsim$ 100 (DePoy 1987). This is consistent with the small hard X-ray luminosity of NGC 1068 (see, e.g., Awaki et al. 1991; Jourdain et al. 1994). The continuum source in NGC 1068 appears to lie behind a thick screen of material with $N_H > 10^{24}$–10^{25} cm^{-2}, and only a few percent of the total hard X-ray luminosity is scattered into our line of sight (Miller et al. 1991; Mulchaey et al. 1992).

A31. NGC 2110 = MCG −01-15-4

NGC 2110 is another object from the sample of X-ray–selected active galaxies with narrow emission lines (Bradt et al. 1978; Ward et al. 1978). A spectrophotometric study of the nuclear region of NGC 2110 by Shuder (1980) revealed the presence of high-ionization lines and possibly a broad component to Hα. No broad component was detected by Veilleux (1991a). VLA maps made at 6 and 20 cm wavelengths (Ulvestad & Wilson 1983) reveal a radio triple radio structure aligned roughly north-south. Emission-line images of NGC 2110 (Wilson et al. 1985; Pogge 1988) show emission extending 15″–20″ in the same general direction as the radio structure.

Rix et al. (1990) were unsuccessful in detecting a broad component to Paβ. However, they used the hard X-ray measurements of NGC 2110 from McClintock et al. (1978) and Marshall et al. (1979) and the well-known proportionality between hard X-ray and broad Hα fluxes among unreddened Seyfert 1 galaxies to predict the intensity of broad Paβ in NGC 2110 under the assumption that this object indeed contains an obscured Seyfert 1 nucleus; they derived $F(\mathrm{Pa}\beta_b) = 4 \times 10^{-14}$ ergs s^{-1} cm^{-2}. This value is only slightly above the upper limit they determined from their spectrum. Our data (Figs. 2*v* and 2*w*) go considerably deeper. The J-band spectrum of NGC 2110 is characterized by very strong [Fe II] λ1.2567 emission. The profile of Paβ appears broad and highly blue asymmetric. This large asymmetry is not observed in the optical profiles (see, e.g., Veilleux 1991a). The profile of Paβ was fitted with a combination of a narrow Gaussian and a broad Gaussian. The results of this fit are listed in Table 3. These parameters should be treated with caution because they are almost certainly affected by the strong stellar continuum in NGC 2110.

An attempt was made to subtract this stellar contribution from the spectrum of NGC 2110. The spectrum of the elliptical galaxy NGC 3379 was used for this procedure. The resulting spectrum was judged only marginally better than the original based on the fact that important residuals still remained at the positions of a number of absorption lines. The profile of Paβ in the continuum-subtracted spectrum is somewhat narrower than in the original data, which makes the fluxes from broad Paβ uncertain. Unfortunately, the stellar continuum of NGC 2110 appears even stronger in the K band (Fig. 2*w*). The emission from H_2 λ2.121 is very strong, but Brγ is strongly affected by structure in the underlying continuum. High-quality spectra of template galaxies will be needed to remove the strong stellar continuum properly in NGC 2110 and reveal the true strength of any obscured BLR.

Taking the broad-line fluxes listed in Table 3 at face value and assuming that Veilleux (1991c) would have detected broad Hα if it had been half the intensity of the narrow line, $E(B-V)_b = 0$, >1.1, or >0.8 based on the value of $F(\mathrm{Br}\gamma_b)/F(\mathrm{Pa}\beta_b)$, and the lower limits on $F(\mathrm{Pa}\beta_b)/F(\mathrm{H}\alpha_b)$ and $F(\mathrm{Br}\gamma_b)/F(\mathrm{H}\alpha_b)$, respectively. Note that the *narrow*-line extinctions derived from the infrared lines are systematically lower than the value derived from the Balmer decrement. This result may be another indication that the fluxes of the *broad* lines have been overestimated.

A32. NGC 7172

NGC 7172 has been tentatively identified with the *HEAO* A-2 hard X-ray source H2158−321 (Marshall et al. 1979). Its nuclear emission spectrum is indicative of excitation by a power-law photoionization source (Sharples et al. 1984). The large

narrow-line Balmer decrement in this galaxy (>6.5; Sharples et al. 1984) indicates substantial obscuration ($A_V > 2.5$ mag) and makes it a good target to search for an obscured broad-line AGN through infrared spectroscopy. The *K*-band spectrum of NGC 7172 is shown in Figure 2*x*. No *J*-band data were taken of this galaxy. The emission around Brγ appears dominated by continuum emission from the underlying stellar component. The H_2 λ2.121 line is barely detected at 2.14 μm, and only an upper limit to the Brγ intensity could be derived. An upper limit of 6×10^{-15} ergs s^{-1} cm^{-2} to the [Fe II] λ1.64 flux was derived by Moorwood & Oliva (1988).

A33. NGC 7212

NGC 7212 is in a system of three interacting galaxies located at a distance of 157 Mpc (Vorontsov-Velyaminov & Arkhipova 1963; Wasilewski 1981). The optical spectrum of this galaxy is typical of Seyfert 2 galaxies (see, e.g., De Robertis & Osterbrock 1986; Veilleux & Osterbrock 1987). Line emission extending over a scale of $\sim 30''$ has been reported (Durret & Warin 1990; Durret 1994). Tran et al. (1992) and Tran (1995a) detected a broad Hα component (FWHM = 3950 km s^{-1}) in the polarized light of NGC 7212. This galaxy was observed in the *K* band (Fig. 2*y*). No obvious broad component is observed in the profile of Brγ. The profile of Brγ is similar to that of the equally strong H_2 λ2.121 feature except for the possible presence of very faint wings in Brγ. We derive a conservatively high upper limit to the broad Brγ flux of 1.3×10^{-15} ergs s^{-1} cm^{-2}. Taken at face value, this flux is nearly an order of magnitude larger than the value predicted from the scattered Hα flux of Tran (1995a, 1995c) and Case B recombination. Emission from He I λ2.058 and H_2 λ2.223 is also visible in our spectrum. The latter feature is unusually broad; it may be part of a blend and is probably also affected by the combination of residuals from atmospheric absorption features and the underlying stellar continuum.

REFERENCES

Aitken, D. K., & Roche, P. F. 1985, MNRAS, 213, 777
Antonucci, R. R. J., & Miller, J. S. 1985, ApJ, 297, 621
Armus, L., Heckman, T. M., & Miley, G. K. 1989, ApJ, 347, 727
Awaki, H., Koyama, K., Inoue, H., & Halpern, J. P. 1991, PASJ, 43, 195
Bailey, J., Axon, D. J., Hough, J. H., Ward, M. J., McLean, I., & Heathcote, S. R. 1988, MNRAS, 234, 899
Bergvall, N., Johansson, L., & Olofsson, K. 1986, A&A, 166, 92
Binette, L., Calvet, N., Canto, J., & Raga, A. C. 1990, PASP, 102, 723
Black, J. H., & Dalgarno, A. 1976, ApJ, 203, 132
Black, J. H., & van Dishoeck, E. F. 1987, ApJ, 322, 412
Blanco, P. R., Ward, M. J., & Wright, G. S. 1990, MNRAS, 242, 4P
Blietz, M., et al. 1994, ApJ, 421, 92
Blumenthal, G. R., Keel, W. C., & Miller, J. S. 1982, ApJ, 257, 499
Bower, G., Wilson, A., Morse, J. A., Gelderman, R., Whittle, M., & Mulchaey, J. 1995, ApJ, 454, 106
Bradt, H. V., et al. 1978, ApJ, 226, L111
Burton, M. G., Hollenbach, D. J., & Tielens, A. G. G. M. 1990, ApJ, 365, 620
Busko, I. C., & Steiner, J. E. 1989, MNRAS, 238, 1479
———. 1992, MNRAS, 258, 306
Cecil, G., Bland, J., & Tully, R. B. 1990, ApJ, 355, 70
Clegg, R., et al. 1991, Gemini, 34, 1
Colina, L. 1993, ApJ, 411, 565
Corbin, M. R., Baldwin, J. A., & Wilson, A. S. 1988, ApJ, 334, 584
Cruz-Gonzalès, J., Carrasco, L., Serrano, A., Guichard, J., Dultzin-Hacyan, D., & Bisiacchi, G. F. 1994, ApJS, 94, 47
Dahari, O., & De Robertis, M. M. 1988, ApJS, 67, 249
DePoy, D. L. 1987, in Infrared Astronomy with Arrays, ed. C. G. Wynn-Williams, E. E. Becklin, & L. H. Good (Honolulu: Univ. Hawaii), 426
De Robertis, M. M. 1987, ApJ, 316, 597
De Robertis, M. M., & Osterbrock, D. E. 1986, ApJ, 301, 727
De Robertis, M. M., & Shaw, R. A. 1990, ApJ, 348, 421
Dopita, M. A., & Sutherland, R. S. 1995, ApJ, 455, 468
Doyon, R., Puxley, P. J., & Joseph, R. D. 1992, ApJ, 397, 117
Doyon, R., Wright, G. S., & Joseph, R. D. 1994, ApJ, 421, 115
Draine, B. T., Roberge, W. G., & Dalgarno, A. 1983, ApJ, 264, 485
Durret, F. 1994, A&AS, 105, 57
Durret, F., & Bergeron, J. 1986, A&A, 156, 51
———. 1988, A&AS, 75, 273
Durret, F., & Warin, F. 1990, A&A, 238, 15
Elias, J. H., Frogel, J. A., Matthews, K., & Neugebauer, G. 1982, AJ, 87, 1029
Evans, I. N., Ford, H. C., Kinney, A. L., Antonucci, R. R. J., Armus, L., & Caganoff, S. 1991, ApJ, 369, L27
Ferland, G. J., & Netzer, H. 1983, ApJ, 264, 105
Ferland, G. J., & Osterbrock, D. E. 1986, ApJ, 300, 658
Fiore, F., Elvis, M., Mathur, S., Wilkes, B. J., & McDowell, J. C. 1993, ApJ, 415, 129
Fischer, J., Geballe, T. R., Smith, H. A., Simon, M., & Storey, J. W. V. 1987, ApJ, 320, 667
Forbes, D. A., & Ward, M. 1993, ApJ, 416, 150
———. 1994, in ASP Conf. Proc. 54, The First Stromlo Symposium: The Physics of Active Galaxies, ed. G. V. Bicknell, M. A. Dopita, & P. J. Quinn (San Francisco: ASP), 429
Forbes, D. A., et al. 1993, ApJ, 406, L11
Gaskell, C. M. 1984, ApJ, 24, L43
Gaskell, C. M., & Ferland, G. J. 1984, PASP, 96, 393
Goldader, J. D., Joseph, R. D., Doyon, R., & Sanders, D. B. 1995, ApJ, 444, 97
Goldader, J. D., Joseph, R. D., Doyon, R., & Sanders, D. B. 1996, ApJ, 474, 104
Goodrich, R. W. 1989, ApJ, 340, 190
———. 1990, ApJ, 355, 88
———. 1992, ApJ, 399, 50
———. 1995, ApJ, 440, 141
Goodrich, R. W., & Osterbrock, D. E. 1983, ApJ, 269, 416
Goodrich, R. W., Veilleux, S., & Hill, G. J. 1994, ApJ, 422, 521 (Paper I)
Gorenstein, P. 1975, ApJ, 198, 95
Greenhill, L., Jiang, D. R., Moran, J. M., Reid, M. J., Lo, K. Y., & Claussen, M. J. 1995, ApJ, 440, 619
Greenhouse, M. A., et al. 1991, ApJ, 383, 164
Gregory, P. C., & Condon, J. J. 1991, ApJS, 75, 1011
Hall, D. N. B., Kleinman, S. G., Scoville, N. Z., & Ridgway, S. T. 1981, ApJ, 248, 898
Halpern, J. P., & Steiner, J. E. 1983, ApJ, 269, L637
Haniff, C. A., Wilson, A. S., & Ward, M. J. 1988, ApJ, 334, 104
Hanson, C. G., Skinner, G. K., Eyles, C. J., & Willmore, A. P. 1990, MNRAS, 242, 262
Hawarden, T. G., Israel, F. P., Geballe, T. R., & Wade, R. 1995, MNRAS, 276, 1197
Heckman, T. M., Beckwith, S., Blitz, L., Skrutskie, M., & Wilson, A. S. 1986, ApJ, 305, 157
Herbst, T. M., Graham, J. R., Beckwith, S., Tsutsui, K., Soifer, B. T., & Matthews, K. 1990, AJ, 99, 1773
Hewitt, A., & Burbidge, G. 1991, ApJS, 75, 297
Hill, G. J., Goodrich, R. W., & DePoy, D. L. 1996, ApJ, 462, 163
Hines, D. C. 1991, ApJ, 374, L9
Israel, F. P., van Dishoeck, E. F., Baas, F., Koornneef, J., Black, J. H., & de Graauw, T. 1990, A&A, 227, 342
Jourdain, E., et al. 1994, A&A, 281, 57
Kawara, K., Nishida, M., & Gregory, B. 1987, ApJ, 321, L35
———. 1990, ApJ, 352, 433
Kawara, K., Nishida, M., & Phillips, M. M. 1989, ApJ, 337, 230
Kawara, K., Nishida, M., & Taniguchi, Y. 1988, ApJ, 328, L41
Kay, L. 1994, ApJ, 430, 196
Kim, D.-C., Sanders, D. B., Veilleux, S., Mazzarella, J. M., & Soifer, B. T. 1995, ApJS, 98, 129
Kinney, A. L., Antonucci, R. R. J., Ward, M. J., Wilson, A. S., & Whittle, M. 1991, ApJ, 377, 100
Kollatschny, W., & Fricke, K. J. 1984, A&A, 135, 171
Königl, A., & Kartje, J. F. 1994, ApJ, 434, 446
Koski, A. T. 1978, ApJ, 223, 56
Krolik, J. H., & Begelman, M. 1986, ApJ, 308, L55
Krolik, J. H., & Lepp, S. 1989, ApJ, 347, 179
Laor, A., & Draine, B. T. 1993, ApJ, 402, 441
Lawrence, A. 1991, MNRAS, 252, 586
Lawrence, A., & Elvis, M. 1982, ApJ, 256, 410
Lepp, S., & McCray, R. 1983, ApJ, 269, 560
Lester, D. F., Carr, J., Joy, M., & Gaffney, N. 1990, ApJ, 352, 544
MacKenty, J. W. 1989, ApJ, 343, 125
Maiolino, R., & Rieke, G. H. 1995, ApJ, 446, 561
Marshall, F. E., et al. 1979, ApJS, 40, 657
Mazzarella, J. M., Gaume, R. A., Aller, H. D., & Hughes, P. A. 1988, ApJ, 333, 168
Mazzarella, J. M., Gaume, R. A., Soifer, B. T., Graham, J. R., Neugebauer, G., & Matthews, K. 1991, AJ, 102, 1241
McClintock, J. E., Bradt, H. V., Canizares, C. R., Kelley, R. L., van Paradijs, J., & Koski, A. T. 1978, Bull. AAS, 10, 424

Miller, J. S., & Goodrich, R. W. 1990, ApJ, 355, 456
Miller, J. S., Goodrich, R. W., & Mathews, W. G. 1991, ApJ, 378, 47
Miller, J. S., & Mathews, W. G. 1972, ApJ, 172, 593
Moorwood, A. F. M., & Oliva, E. 1988, A&A, 203, 278
———. 1990, A&A, 239, 78
Moshir, M., et al. 1992, Explanatory Supplement to the IRAS Faint Source Survey, Version 2 (Pasadena: JPL)
Mountain, C. M., Robertson, D. J., Lee, T. J., & Wade, R. 1990, Instrumentation in Astronomy VII, ed. D. L. Crawford (Proc. SPIE, 1235), 25
Mouri, H., Kawara, K., & Taniguchi, Y. 1993, ApJ, 406, 52
Mouri, H., Nishida, M., Taniguchi, Y., & Kawara, K. 1990, ApJ, 360, 55
Mouri, H., & Taniguchi, Y. 1995, ApJ, 449, 134
Mouri, H., Taniguchi, Y., & Kawara, K. & Nishida, M. 1989, ApJ, 346, 73
Mulchaey, J. S., et al. 1994, ApJ, 436, 586
Mulchaey, J. S., Mushotzky, R. F., & Weaver, K. A. 1992, ApJ, 390, L69
Nakajima, T. Carleton, N. R., & Nishida, M. 1991, ApJ, 375, L1
Nandra, K., et al. 1993, MNRAS, 260, 504
Nandra, K., & Pounds, K. A. 1992, Nature, 359, 215
Netzer, H., & Laor, A. 1993, ApJ, 404, L51
Neugebauer, G., Oke, J. B., Becklin, E. E., & Matthews, K. 1979, ApJ, 230, 79
Oliva, E., & Moorwood, A. F. M. 1990, ApJ, 348, L5
Osterbrock, D. E. 1977, ApJ, 215, 733
———. 1985, PASP, 97, 25
———. 1989, Astrophysics of Gaseous Nebulae and Active Galactic Nuclei (Mill Valley: University Science Books)
Osterbrock, D. E., & Dahari, O. 1983, ApJ, 273, 478
Osterbrock, D. E., & Martel, A. 1992, PASP, 101, 76
———. 1993, ApJ, 414, 552
Osterbrock, D. E., & Shaw, R. A. 1988, ApJ, 327, 89
Osterbrock, D. E., Tran, H. D., & Veilleux, S. 1992, ApJ, 389, 196
Perek, L., & Kohoutek, L. 1967, Catalogue of Galactic Planetary Nebulae (Prague: Academia)
Phillips, M. M., Charles, P. A., & Baldwin, J. A. 1983, ApJ, 266, 485
Phinney, E. S. 1989, in IAU Symp. 136, The Center of the Galaxy, ed. M. Morris (Dordrecht: Kluwer), 543
Pier, E. A., & Krolik, J. H. 1992a, ApJ, 399, L23
———. 1992b, ApJ, 401, 99
———. 1993, ApJ, 418, 673
Pogge, R. W. 1988, ApJ, 332, 702.
———. 1989, ApJ, 345, 730
Pogge, R. W., & De Robertis, M. M. 1993, ApJ, 404, 563
Puxley, P. J., Hawarden, T. G., & Mountain, C. M. 1990, ApJ, 364, 77
Puxley, P. J., Lumsden, S. L., Brand, P. W. J. L., & Doyon, R. 1994, MNRAS, 270, L7
Rieke, G. J., & Lebofsky, M. J. 1985, ApJ, 288, 618
Rix, H.-W., Carleton, N. P., Rieke, G., & Rieke, M. 1990, ApJ, 363, 480
Roche, P. F., & Aitken, D. K. 1985, MNRAS, 215, 425
Roche, P. F., Aitken, D. K., Phillips, M. M., Whitmore, B. 1984, MNRAS, 207, 35
Roche, P. F., Aitken, D. K., Smith, C. H., & James, S. D. 1986, MNRAS, 218, 21P
Rotaciuc, V., et al. 1991, ApJ, 370, L23
Rudy, R. J., Cohen, R. D., Rossano, G. S., Puetter, R. C., & Chapman, S. C. 1989, ApJ, 341, 120
Ruiz, M., Rieke, G. H., & Schmidt, G. D. 1994, ApJ, 423, 608
Sandage, A., & Tammann, G. A. 1987, A Revised Shapley-Ames Catalog of Bright Galaxies (2d ed.; Washington: Carnegie Inst. of Washington)
Sanders, D. B., Phinney, E. S., Neugebauer, G., Soifer, B. T., & Matthews, K. 1989, ApJ, 347, 29
Sanders, D. B., Soifer, B. T., Elias, J. H., Neugebauer, G., & Mathews, K. 1988, ApJ, 328, L35
Scoville, N. Z., Hall, D. N. Z., Kleinman, S. G. & Ridgway, S. T. 1982, ApJ, 253, 136
Sharples, R. M., Longmore, A. J., Hawarden, T. G., & Carter, D. 1984, MNRAS, 208, 15
Shields, J. C. 1993, ApJ, 419, 181
Shields, J. C., & Filippenko, A. V. 1988, ApJ, 332, L55
———. 1990, AJ, 100, 1034
Shuder, J. M. 1980, ApJ, 240, 32
Shuder, J. M., & Osterbrock, D. E. 1981, ApJ, 250, 55
Shull, J. M., & Hollenbach, D. J. 1978, ApJ, 220, 525
Sternberg, A. 1988, ApJ, 332, 400
Sternberg, A., & Dalgarno, A. 1989, ApJ, 338, 197
Storchi-Bergmann, T., Mulchaey, J. S., & Wilson, A. S. 1992a, ApJ, 395, L73
Storchi-Bergmann, T., Wilson, A. S., & Baldwin, J. A. 1992b, ApJ, 396, 45
Tadhunter, C., & Tsvetanov, Z. 1989, Nature, 341, 422
Taniguchi, Y., Kameya, O., Nakai, N., & Kawara, K. 1990, ApJ, 358, 132
Taylor, D., Dyson, J. E., & Axon, D. J. 1992, MNRAS, 255, 351
Terlevich, R. J., et al. 1991, ApJS, 91, 285
Thompson, R. I. 1995, ApJ, 445, 700
Thompson, R. I., Lebofsky, M. J., & Rieke, G. H. 1978, ApJ, 222, L49
Tran, H. D. 1995a, ApJ, 440, 565
———. 1995b, ApJ, 440, 578
———. 1995c, ApJ, 440, 597
Tran, H. D., Miller, J. S., & Kay, L. E. 1992, ApJ, 397, 452
Tsvetanov, Z., & Walsh, J. R. 1992, ApJ, 386, 485
Turner, T. J., et al. 1993a, ApJ, 407, 556
Turner, T. J., Nandra, K., George, I. M., Fabian, A. C., & Pounds, K. A. 1993b, ApJ, 419, 127
Turner, T. J., Weaver, K. A., Mushotzky, R. F., Holt, S. S., & Madejski, G. M. 1991, ApJ, 381, 85
Ulvestad, J. S., Antonucci, R. R. J., & Goodrich, R. W. 1995, AJ, 109, 81
Ulvestad, J. S., & Wilson, A. S. 1983, ApJ, 264, L7
———. 1984a, ApJ, 278, 544
———. 1984b, ApJ, 285, 439
———. 1989, ApJ, 343, 659
Unger, S. W., Pedlar, A., Axon, D. J., Whittle, M., Meurs, E. J. A., & Ward, M. J. 1987, MNRAS, 228, 671
Unger, S. W., Taylor, K., Pedlar, A., Ghataure, H., Penston, M. V., & Axon, D. J. 1989, in IAU Symp. 134, Active Galactic Nuclei, ed. D. E. Osterbrock and J. S. Miller (Mill Valley, Ca: University Science Books), 331
van der Werf, P. P., Genzel, R., Krabbe, A., Blietz, M., Lutz, D., & Drapatz, S. 1993, ApJ, 405, 522
Veilleux, S. 1991a, ApJS, 75, 357
———. 1991b, ApJS, 75, 383
———. 1991c, ApJ, 369, 331
Veilleux, S., Cecil, G., Bland-Hawthorn, J., Tully, R. B., Filippenko, A. V., & Sargent, W. L. W. 1994, ApJ, 433, 48
Veilleux, S., & Osterbrock, D. E. 1987, ApJS, 63, 297
Véron, P., Lindblad, P. O., Zuiderwijk, E. J., Véron, M.-P., & Adam, G. 1980, A&A, 87, 245
Vorontsov-Velyaminov, B. A., & Arkhipova, V. P. 1963, Morphological Catalogue of Galaxies, Part III (Trudy Astr. Inst. Sternberg 33), 68
Vrtilek, J. M., & Carleton, N. P. 1985, ApJ, 294, 106
Ward, M. J., Elvis, M., Fabbiano, G., Carleton, N. P., Willner, S. P., & Lawrence, A. 1987, ApJ, 315, 74
Ward, M. J., Wilson, A. S., Penston, M. V., Elvis, M. Maccacaro, T., & Tritton, K. P. 1978, ApJ, 223, 788.
Wasilewski, A. J. 1981, PASP, 93, 560
Wehrle, A. E., & Morris, M. 1988, AJ, 95, 1689
Whitford, A. E. 1958, AJ, 63, 201
Whittle, M. 1985, MNRAS, 213, 1
———. 1992, ApJS, 79, 49
Whittle, M., Pedlar, A., Meurs, E. J. A., Unger, S. W., Axon, D. J., & Ward, M. J. 1988, ApJ, 326, 125
Wilson, A. S., & Baldwin, J. A. 1989, AJ, 98, 2056
Wilson, A. S., Baldwin, J. A., & Ulvestad, J. S. 1985, ApJ, 291, 627
Wilson, A. S., Braatz, J. A., Heckman, T. M., Krolik, J. H., & Miley, G. K. 1993, ApJ, 419, L61
Wilson, A. S., Haniff, C. A., & Ward, M. J. 1988, ApJ, 334, 121
Wilson, A. S., Penston, M. V., Fosbury, R. A. E., & Boksenberg, A. 1976, MNRAS, 177, 673
Wilson, A. S., & Tsvetanov, Z. I. 1994, AJ, 107, 1227
Wilson, A. S., & Willis, A. G. 1980, ApJ, 240, 429